Modeling Solvatochromic Shifts Using the Orbital-Free Embedding Potential at Statistically Mechanically Averaged Solvent Density

Jakub W. Kaminski,[†] Sergey Gusarov,[‡] Tomasz A. Wesolowski,*[,†] and Andriy Kovalenko[‡,§]

Département de Chimie Physique, Université de Genève, 30 quai Ernest-Ansermet, CH-1211 Genève 4, Switzerland, National Research Council of Canada. National Institute for Nanotechnology, 421 Saskatchewan Drive T6G 2M9 Edmonton, Canada, and Department of Mechanical Engineering, University of Alberta, T6G 2G8 Edmonton, Canada

Received: January 7, 2010; Revised Manuscript Received: March 23, 2010

The correspondence between the exact embedding potential and the pair of the electron densities—that of the embedded molecule and that of its environment [Wesolowski and Warshel, *J. Phys. Chem.* **1993**, *97*, 8050]—is used to generate the average embedding potential and to subsequently calculate the solvatochromic shifts in a number of organic chromophores in solvents of various polarities. The averaged embedding potential is evaluated at a fictitious electron density of the solvent, which is obtained by means of "dressing up" with electrons the classical site distributions derived from the statistical-mechanical, 3D molecular theory of solvation (aka 3D-RISM method) [Kovalenko In *Molecular Theory of Solvation*; Hirata, Ed.; Understanding Chemical Reactivity; 2003, Vol 24], self-consistently coupled with the electronic structure of the solute. The proposed approach to modeling solvatochromic shifts can be situated between the implicit and explicit type of models for the solvent. Numerical examples are given for the lowest-lying $n \rightarrow \pi^*$ and $\pi \rightarrow \pi^*$ excitations.

1. Introduction

Solvents are known to affect such physicochemical properties of molecules as geometry, conformational equilibria, reaction rates, as well as their UV-vis, IR, or NMR spectra, for instance.[1] A large number of computer modeling techniques were developed to study solvent effects on such properties. In the most simple ones, the environment of a solvated molecule is treated implicitly. It is represented as a cavity in a homogeneous dielectric that gives rise to the reaction field (for recent reviews see refs 2 and 3). The implicit models have been used extensively and adequately describe the solvent effects on many properties. One of their drawbacks is neglecting specific intermolecular interactions such as hydrogen bonds. Explicit solvent models, where both the solvent as well as the environment are described at the level of nonrelativistic Schrödinger equation in Born−Oppenheimer approximation, can be situated at another end. In principle, such models can describe almost every property of solvated molecules, but their practical applications are limited for two principal reasons: the fast increase of the computational cost with the increase of the size of the system and the need for averaging due to the statistical nature of the solvent. The explicit models can be simplified by treating the whole quantum mechanical system comprising the solvated molecule on one hand and the solvent molecules on another hand in a hybrid way, in which the system of interest is described at the quantum-mechanical (QM) level, and solvent at some lower level of description. Such schemes are known under such labels as QM/QM[4] or QM/MM.[5] Another group of approaches, where the solvent is described by means of site probabilities, can be situated between implicit and explicit levels. The statistical-mechanical molecular theory of liquids, three-dimensional reference interaction site model (3D-RISM)[6] in particular, provides a formal framework to obtain the probabilities (referred to in the present work as site distributions) of finding a solvent molecule at a given position and orientation with respect to the solute. At the 3D-RISM level, the solvent is not uniform and the specific interactions are accounted for as modifications of the 3D site distributions, which are statistical quantities. The interactions between the subsystem described at the QM level and its 3D-RISM environment are taken into account in a straightforward manner by the electrostatic potential derived from 3D-RISM site distributions.

Turning back to the QM/MM and QM/QM models, the possible strategy to include the solvent in the calculation of molecular properties is based on the embedding strategy, in which only a selected part of the whole system is described using QM descriptors, whereas the remaining part (environment) is taken into account by means of a special potential (embedding potential) added to the gas phase Hamiltonian. The most commonly used embedding potentials comprise terms originating in the theory of intermolecular interactions. In the simplest version, the embedding potential comprises only terms representing classical Coulomb interactions, which are frequently further simplified using truncated multipole expansion, whereas more refined potentials also account for solvent polarization through a reaction field (discrete or continuous)[4,5,7−9] (for extensive review, see refs 2, 3, 10, and 11). The Hohenberg−Kohn variational principle provides another strategy to construct the embedding potential in a system-independent way.[12−14] Wesolowski and Warshel[12] showed that the optimal (i.e., minimizing the Hohenberg−Kohn energy functional[15]) embedding potential is uniquely determined by the pair of the electron densities—that of the investigated embedded system ($\rho_A(\vec{r})$) and that of its environment ($\rho_B(\vec{r})$). Using density functionals for: (i) the kinetic energy of noninteracting reference system ($T_s[\rho]$) and (ii) the exchange-correlation energy ($E_{xc}[\rho]$), known in the Kohn−Sham formulation[16] of

* To whom correspondence should be addressed. E-mail: tomasz.wesolowski@unige.ch.
† Université de Genève.
‡ National Institute for Nanotechnology.
§ University of Alberta.

10.1021/jp100158h
Published on Web 04/26/2010

density functional theory and their constrained search definitions,[17] this correspondence reads:

$$v_{\mathrm{emb}}^{\mathrm{KSCED}}[\rho_{\mathrm{A}},\rho_{\mathrm{B}};\vec{r}] = v_{\mathrm{ext}}^{\mathrm{B}}(\vec{r}) + \int \frac{\rho_{\mathrm{B}}(\vec{r}')}{|\vec{r}'-\vec{r}|}\mathrm{d}\vec{r}' + v_{\mathrm{xc}}^{\mathrm{nad}}[\rho_{\mathrm{A}},\rho_{\mathrm{B}}](\vec{r}) + v_{t}^{\mathrm{nad}}[\rho_{\mathrm{A}},\rho_{\mathrm{B}}](\vec{r}) \quad (1)$$

where:

$$v_{t}^{\mathrm{nad}}[\rho_{\mathrm{A}},\rho_{\mathrm{B}}](\vec{r}) = \left.\frac{\delta T_{\mathrm{s}}[\rho]}{\delta\rho}\right|_{\rho=\rho_{\mathrm{A}}+\rho_{\mathrm{B}}} - \left.\frac{\delta T_{\mathrm{s}}[\rho]}{\delta\rho}\right|_{\rho=\rho_{\mathrm{A}}} \quad (2)$$

and

$$v_{\mathrm{xc}}^{\mathrm{nad}}[\rho_{\mathrm{A}},\rho_{\mathrm{B}}](\vec{r}) = \left.\frac{\delta E_{\mathrm{xc}}[\rho]}{\delta\rho}\right|_{\rho=\rho_{\mathrm{A}}+\rho_{\mathrm{B}}} - \left.\frac{\delta E_{\mathrm{xc}}[\rho]}{\delta\rho}\right|_{\rho=\rho_{\mathrm{A}}} \quad (3)$$

are nonadditive kinetic energy and exchange correlation potentials, respectively. Term $v_{\mathrm{ext}}^{\mathrm{B}}(\vec{r})$ is external potential generated by nuclei of the environment.

The above equation provides system-independent, exact expression for the universal embedding potential coupling two subsystems. The Kohn−Sham-like equations for embedded orbitals ϕ_{A}:

$$\left[-\frac{1}{2}\nabla^2 + v_{\mathrm{eff}}^{\mathrm{KS}}[\rho_{\mathrm{A}},\vec{r}] + v_{\mathrm{eff}}^{\mathrm{KSCED}}[\rho_{\mathrm{A}},\rho_{\mathrm{B}};\vec{r}]\right]\phi_i^{\mathrm{A}} = \varepsilon_i^{\mathrm{A}}\phi_i^{\mathrm{A}} \quad i = 1, N^{\mathrm{A}} \quad (4)$$

provide a self-consistent way to minimize of the energy of the total system for a given $\rho_{\mathrm{B}}(\vec{r})$, that is, to optimize the embedded electron density in the subsystem A ($\rho_{\mathrm{A}} = 2\sum_i^{N_{\mathrm{A}}}|\phi_i^{\mathrm{A}}|^2$). For the complete description of the formalism based on the above equation see ref 18. The environment is described only by its electron density ρ_{B}, which is an assumed quantity. No additional information about orbital structure of solvent is required. Note also, that density ρ_{B} remains constant during iterative process of solving eq 4. For this reasons we commonly refer to such method as orbital-free embedding (OFE) or frozen density embedding (FDE). The label KSCED in eq 4 stands for the Kohn−Sham equations with constrained electron density and is introduced to indicate that the total effective potential in eq 4 differs from the one in the Kohn−Sham equations.

Although $v_{\mathrm{emb}}^{\mathrm{KSCED}}[\rho_{\mathrm{A}},\rho_{\mathrm{B}};\vec{r}]$ was derived for embedding a reference system of noninteracting electrons, the same or very similar correspondence between the optimal embedding potential and the pair of electron densities ρ_{A} and ρ_{B} exist for embedding other quantum mechanical objects such as embedded wave function[13] or embedded one-particle reduced density matrix.[14] The results of practical applications of the embedding potential given in eq 1 in combination with wave function based models are encouraging.[19−21] Considering applications of eq 4, various studies are available in the literature.[22,28−30] In all of them the quality of the results hinges on the choice of the density ρ_{B} corresponding to the environment. Owing to the fact that this density is an assumed quantity, a variety of theoretical methods working at different level of approximation can be applied to obtain ρ_{B}. In our common practice, depending on the studied system or on the observable of interest, we adopted several strategies to generate ρ_{B}, all of them based on the Kohn−Sham formalism. The lowest level of description of the electron density of the environment is to construct ρ_{B} as the sum of the atomic or molecular densities of atoms or molecules in the environment.[34] This level might be adequate if neither the solvent molecules nor the embedded molecule are polar. This model can be further refined if $\rho_{\mathrm{B}}(\vec{r})$ is obtained in one Kohn−Sham calculation for the whole environment but with the absence of the embedded molecule. Such treatment of the solvent is adequate only if the electron density of the environment is not significantly modified by the presence of the solute (electronic polarization of the solvent molecules, for instance). In such a way, ρ_{B} includes the interactions between molecules constituting it: however, it does not account for the polarization of the environment by the embedded subsystem. This can be partly overcome by performing the Kohn−Sham calculations of the whole environment including point charges or dipole moments representing the field of embedded system, leading to prepolarized ρ_{B}, that is, to use as ρ_{B} the electron density of the molecules in the environment, which is polarized by the electric field generated by the solute. The most accurate approach is not to do any assumptions concerning ρ_{B} but to obtain it variationally, that is, to find such a pair of densities ρ_{A} and ρ_{B}, that minimizes the Cortona functional for the total energy.[35] Such minimization can be performed using the freeze-and-thaw algorithm.[36] In freeze-and-thaw calculations, both the embedded molecule and the environment are treated on equal footing and the notion of embedded system and the environment is not applicable. In our applications of eq 4, the freeze-and-thaw calculations are used to verify the adequacy of simplifications made for $\rho_{\mathrm{B}}(\vec{r})$ in large scale simulations. Numerical examples of the convergence of the calculated properties along the above hierarchy of methods to generate the electron density of the environment can be found in our previous works on ligand-fields splitting of f-levels in lanthanide impurities[30] or on solvent effect on the UV-vis spectra of organic chromophores.[28,29] In the discussed above schemes, $\rho_{\mathrm{B}}(\vec{r})$ has always a quantum-chemical origin and can be associated with some molecular system at a given geometry. In the present work, an alternative approach to generate density $\rho_{\mathrm{B}}(\vec{r})$ is introduced. The quantum-chemical descriptors for the electron density of the environment are not used at all. Instead, the electron density of the environment is obtained using the classical-theory-of-liquids derived site distributions, which are subsequently "dressed up" with electrons. The resulting electron density—the averaged electron density of the solvent denoted with $\langle(\rho_{\mathrm{B}}(\vec{r}))\rangle$ throughout this work—is used subsequently in the evaluation of the orbital-free embedding potential given in eq 1. We exploit here explicitly the fact that eq 1 provides an unique correspondence between the exact embedding potential and charge densities even if $\rho_{\mathrm{B}}(\vec{r})$ is not obtained from any quantum mechanical method.[12−14] $\langle(\rho_{\mathrm{B}}(\vec{r}))\rangle$ cannot be associated with the electron density of any molecular system as it represents a local function giving the ensemble averaged probability to find an electron in a given place in space. This is an entirely new strategy in the orbital-free embedding calculations. In the subsequent discussion, we will refer to such potential as the "average orbital-free embedding potential" or just "average embedding potential". It is worthwhile to recall that the idea of averaging the potential generated by the solvent is not new in molecular simulations.[31−33,138] The name—averaged solvent electrostatic potential—used for such a potential in ref 31, for instance, illustrates clearly the difference between such averaged potentials and the average embedding potential in the present work, where it is not the potential that is averaged but

the solvent charge density, and where the potential in question includes also a nonelectrostatic part. The difference between averaging the potential directly or calculating it at the averaged solvent charge density arises from the fact that the potential given by eq 1 is nonlinear in ρ_B.[94]

The stress on the embedding potential not just on the expression for the total energy of an embedded system is made here in view of our interest in properties directly related to the electronic structure. The target property analyzed in the present work is the shift of the absorption band center of a chromophore induced by the interactions with the solvent molecules (solvatochromic shift). A straightforward approach to simulate solvatochromic shifts uses an ensemble representing the solvent and evaluation of the excitation energy for each configuration in the ensemble. The quality of the spectral shifts obtained in this way depends on the quality of the evaluated excitation energy at each geometry but also on the used sample of geometries of the solvent. Concerning the latter factor, molecular dynamics simulations are frequently used for this purpose.[28,29,37,38] Such simulations allow one to obtain not only the spectral shifts but also the shape of the absorption bands.

As far as the former factor is concerned, the spectral shifts can be obtained following the linear-response time-dependent density-functional-theory (LR-TDDFT) strategy[39] applied for the embedded orbitals (i.e., orbitals derived from eq 4). For a description of the details of such calculations and benchmark results, see refs 22 and 40. The absorption band in such a case is just:

$$I(\omega) = \sum_i f_i[\rho_B(\{R_j^B\})]\delta(\omega - \omega_i[\rho_B(\{R_j^B\})]) \qquad (5)$$

where f_i and ω_i are the oscillator strength and the resonance frequency for the transition i, $\{R_j^B\}$ denotes the positions of the nuclei in the environment (j changes from 1 to the total number of atoms in the environment), f_i and ω_i are functionals of the electron density $\rho_B(\vec{r})$ of the environment of the chromophore, and δ is the Dirac delta function. Note that the square brackets in the above equation denote the fact that the evaluated quantity is a function of the electron density, that is, it is uniquely determined by the function inside the square brackets.

For an environment of a flexible structure, such as the molecules surrounding a chromophore in the liquid phase, the picture based on single arrangement of nuclei in the environment ($\{R_j^B\}$) is not adequate. Due to difference in time-scale of the electronic transitions and the motions of the nuclei in the environment, eq 5 can be generalized by averaging over the ensamble of configurations $\{R_j^{B(n)}\}$, where n is the index for the configurations of the nuclei in the solvent.

$$I(\omega) = \langle \sum_i f_i[\rho_B(\{R_j^{B(n)}\})]\delta(\omega - \omega_i[\rho_B(\{R_j^{B(n)}\})])\rangle_n \qquad (6)$$

In our previously reported work on acetone[28] and on aminocoumarin,[29] the ensemble of structures of the solvent $\{R_j^{B(n)}\}$ was obtained from either classical, that is, pair-potential-based or QM (Car−Parrinello[41]) molecular dynamics simulations. For such chromophores, which are characterized by broad and diffuse absorption bands, the strategy based on eq 6 implies, however, averaging over a large number of orientations, otherwise the sample of the used configurations is not representative. The CPU costs of the calculation of the excitation energy at one configuration of the solvent can be significantly reduced by using the aforementioned hierarchy of methods to generate $\rho_B(\vec{r})$ in a simplified manner. In practice, it is the number of configurations used to represent the solvent, that determines the overall CPU costs of the simulation of the absorption band.

In the present work, we consider an alternative strategy to obtain the spectral shifts. Instead of averaging f_i and ω_i over a large number of configurations, these quantities are evaluated for a fictitious density $\langle\rho_B(\vec{r})\rangle$, which is the ensemble averaged electron density of the environment. Simulating the absorption bands by performing the orbital-free embedding calculations of the excitation energy at the averaged solvent density $\langle\rho_B(\vec{r})\rangle$ is proposed here principally as the method to overcome the difficulty in obtaining the excitation energy for a sufficient number of solvent configurations to represent adequately the statistical ensemble. This problem arises from the fact that the overall computational costs of the simulation increases linearly with the number of configurations used in the averaging procedure and is proportional to the computational cost of the evaluation of the excitation energy for a given configuration of the solvent.

The strategy to obtain the averaged quantities applied in the present work corresponds to the following approximation:

$$\begin{aligned} I(\omega) &= \langle \sum_i f_i[\rho_B(\{R_j^{B(n)}\})]\delta(\omega - \omega_i[\rho_B(\{R_j^{B(n)}\})])\rangle_n \\ &\approx \sum_i f_i[\langle\rho_B\rangle]\delta(\omega - \omega_i[\langle\rho_B\rangle]) \end{aligned} \qquad (7)$$

Note that the averaged electron density of the solvent ($\langle\rho_B\rangle$) depends on the position, but it does not involve any explicit variables describing the geometry of the solvent molecules. Simplifying the description of the environment by abandoning the atomistic treatment of the ensemble of the solvent and using, instead, the average density of the solvent $\langle\rho_B(\vec{r})\rangle$ in the evaluation of excitation energy aims, therefore, at obtaining better averages. It is, however, an approximation introduced in eq 7. Moreover, $\langle\rho_B(\vec{r})\rangle$ provides a less complete descriptor of the solvent as the statistical ensemble of configurations. For instance, the shape of the absorption band cannot be obtained from such calculations but only individual lines (see eq 7). Finally, the position of the absorption band depends on the quality of the used $\langle\rho_B(\vec{r})\rangle$.

Equation 7 is the main new element in the computational protocol for calculating the solvatochromic shifts proposed in this work, and it is also one of the two main approximations (the other is the procedure to obtain $\langle\rho_B(\vec{r})\rangle$ described in the subsequent sections). Besides the fact that the approximation given in eq 7 cannot describe the shapes of the absorption lines, even the position of the absorption band can be affected by this approximation. Averaging the electron density of the solvent neglects the coupling between the instantaneous electronic structure of the solute and the structure of the solvent. Such coupling can be expected to play an important role for nonpolar but polarizable solutes in polar solvents. The unique correspondence between the pair of electron densities (solvent and solute) and the embedding potential given in eq 1 brings also another important consequence for the LR-TDDFT calculations, which hinge on functional derivatives of the effective potential. Such correspondence makes it possible not only to replace averaging the potential by the potential calculated at the

average density $\langle\rho_B(\vec{r})\rangle$ but also do the same for the response kernel, that is, instead of averaging the kernel, calculation of the kernel at $\langle\rho_B(\vec{r})\rangle$.

In the present work, we obtain $\langle\rho_B(\vec{r})\rangle$ not from QM calculations, but by "dressing up" with electrons the classical site distributions (quantities related to nuclear positions rather than to electrons) obtained from a particular variant of the Ornstein−Zernike equations of the statistical theory of liquids, that is, the 3D reference interacting site model with the Kovalenko-Hirata closure approximation (3D-RISM-KH).[6] Such densities are subsequently "dressed up" with electron densities leading to the average electron density of the solvent, which is denoted with $\langle\rho_B(\vec{r})\rangle$. The overall computational protocol combining: the average electron density of the liquid obtained as dressed up 3D-RISM-KH site distributions, orbital-free embedding with the applied approximants in eq 4, and the evaluation of the spectral shifts from linear-response calculations for embedded subsystem, will be labeled with OFE/RISM for the sake of simplicity in the present work.

Several chromophores, for which the strong dependency of the UV-vis spectra bands on the surrounding media is known, are chosen for the study. Our previous works validated the use of the orbital-free embedding strategy to obtain hydrogen-bonding-induced shifts of the excitation energies in the case of a rigid environment of the chromophore. The present work rather addresses the issue of efficient calculation of averages for flexible environments such as the considered solvents.

2. Methodology

2.1. Spectral Shifts from the Orbital-Free Embedding Calculations at a Rigid Geometry of the Environment. The applications of the orbital-free embedding potential to evaluate the complexation-induced shifts of the low-lying excitations in organic chromophores follows the same framework as the one introduced in ref 40 and subsequently applied in several works.[22,28,29] In this framework, the LR-TDDFT strategy to obtain electronic excitation is applied not for the Kohn−Sham orbitals and the Kohn−Sham effective potential but for the corresponding quantities in eq 4, that is, the embedded orbitals and the total effective potential. Such a computational scheme is especially suited for modeling the complexation-induced shifts and not the absolute values of the excitation energies because the latter depend on the quality of the excitation energy for the isolated chromophore derived from LR-TDDFT. The straightforward application of the supermolecular strategy, that is, evaluation of the shifts as the difference between the LR-TDDFT excitation energies calculated for the chromophore in the complex and for the isolated chromophore, hinges on the cancellation of errors in the effective potential and in its functional derivative (response kernel). The errors in these quantities result in the errors in excitation energies of the magnitude reaching the 0.1−0.2 eV,[23] that is, the same order of magnitude as the investigated spectral shifts. The situation is quite different in the orbital-free embedding case. Owing to the unique correspondence between the pair of the electron densities (chromophore and its environment) and the embedding potential (eq 1), also the embedding component of the response kernel is uniquely determined by this pair of densities. The errors in the calculated spectral shifts at a given rigid geometry of the environment arise from the fact that nonelectrostatic terms in eq 1 are defined as density functionals of unknown analytical form and they are evaluated using approximants. In the hydrogen-bonded complexes, the electrostatic part of the orbital-free embedding potential dominates and the errors in the part evaluated using approximants can be expected to play a smaller relative role. As a consequence, the errors in the spectral shifts can be expected to be smaller than the ones in the absolute excitation energies. Indeed, numerical results confirm this.[22,40] The absolute values of the excitation energies in the complex are as good as their counterparts for the isolated component and can vary depending on the choice for the approximant for the exchange-correlation potential and its functional derivative. The applied approach is by construction only applicable for excitations localized in the chromophore.[46] Otherwise, the nondynamical (frequency dependent) response of the electron density in the environment has to be taken into account. In the case of localized excitations, the embedding strategy offers a serious advantage over a possible alternative, in which the LR-TDDFT calculations are applied for the whole system including the chromophore and the environment. Such calculations not only scale unfavorably with the size of the environment but are known to suffer from artificial low lying excitations.[28,42−45] The importance of such spurious excitations increases with increasing size of the system. Restricting the orbital space to the confined system thus provides a practical remedy for this problem.

The applied scheme to evaluate the spectral shifts in the case of a structurally rigid environment of a chromophore is based on a number of approximations/simplifications of various nature. Some of them have clear physical interpretation, others are due to the use of approximants for the density functionals defined in the exact embedding theory, and some are of purely technical character. They are summarized below:

NDRE: Neglect of the Dynamic Response in the Environment. By construction, neither in solving eq 4 nor in solving response equations in LR-TDDFT is the electron density ρ_B allowed to vary. It is fixed (frozen) at some initial value. As the consequence, the dynamic response of the environment to the electron excitation is neglected. Only virtual embedded orbitals (ϕ_A in eq 4), which are localized on chromophores, are used to construct its response. Therefore, only interfaces in which the environment does not absorb in the considered spectral range can be accurately described. In the considered cases, NDRE is an adequate approximation as confirmed in our dedicated analysis of complexation induced shifts in similar systems.[22] NDRE can be lifted by using the full framework combining the subsystem formulation of DFT with LR-TDDFT.[39] In practice, the most efficient way to lift this simplification is to allow for coupled responses (method labeled as FDEc in ref 46).

Use of the Same Geometry of the Solute with- and without the Environment. It was already shown in previous studies, that influence of the solvent on the geometry and absorption spectrum of the solute can be very important.[24,25] For the examples provided in this work, the solvatochromic shifts were evaluated assuming the same geometry of the solute in each of the considered solvents. This is obviously an approximation. Dedicated studies on solvatochromic shifts in a representative sample of the chromophores indicate that these effects affect the shifts in vertical excitation energy on average by 20%.[26] This bring us to another approximation made commonly in the simulations of the solvatochromic shifts, where it is assumed that the shifts in the maxima of the absorption bands from the gas phase to a solvent (or between two different solvents) is the same as the shifts in the vertical excitation energy. In this work, the same assumption is made (for detailed analysis see ref 27).

Use of Approximants Instead of the Exact Density Functionals. In practical calculations, the kinetic end exchange-correlation components of the effective potential in eq 4 and of

the response kernel are obviously not evaluated exactly but by means of some approximants to these quantities. The choices for the approximants made for these quantities were tested previously for similar systems.[22,40] The term $\upsilon_t^{\mathrm{nad}}[\rho_A, \rho_B](\vec{r})$ in eq 4 vanishes with the increasing distance from chromophore. The applied approximant for this term satisfies this exact condition. It can be expected, therefore, that the asymptotic behavior of the embedding potential used in practical calculations is correct. Note that the electrostatic terms in eq 1 are exact. In our previously reported study on the DNA base pairs,[40] it was shown that maximum deviation in the shifts of excitation energies obtained applying embedding strategy does not exceed 0.05 eV when compared to a supermolecular approach. The respective deviation with the experimental result was recently established to not exceed 0.04 eV.[22] The magnitude of such discrepancies is, however, smaller than the magnitude of the solvatochromic shifts in most of the cases analyzed in the present work. For these reasons we will not discuss solvent-induced shifts of absorption bands smaller than these values.

Numerical Implementation. All the calculations are made using finite basis sets, numerical grid integrations, and the iterative procedure to diagonalize the response matrix in LR-TDDFT. The choices made for these numerical parameters (see the Computational Details section) are based on the accumulated numerical experience with the used solvent and are expected to affect the calculation spectral shifts less than the aforementioned approximants and approximations.

The overall accuracy of the solvatochromic shifts is not only determined by the above factors, which determine the accuracy of spectral shifts at a rigid environment, but also on the quality of the description of the statistically fluctuating solvent. In particular, it is affected by the main approximation of this work given in eq 7. The factors affecting the quality of the average electron density of the environment ($\langle\rho_B(\vec{r})\rangle$) used in eq 7 will be overviewed in the subsequent sections.

2.2. Classical Site Distributions from the 3D-RISM-KH Theory. The classical site distributions for a molecular solvent around a solute of arbitrary shape are obtained by using the 3D-RISM-KH molecular theory of solvation.[6,47] The 3D-RISM integral equation can be derived from the six-dimensional, molecular Ornstein−Zernike integral equation[48] for the solute−solvent correlation functions by averaging out the orientation degrees of freedom of solvent molecules while keeping the orientation of the solute macromolecule described at the 3D level.[6,47] It has the form

$$h_\gamma^{\mathrm{uv}}(\vec{r}) = \sum_\alpha \int \mathrm{d}\vec{r}\; c_\alpha^{\mathrm{uv}}(\vec{r} - \vec{r}')\chi_{\alpha\gamma}^{\mathrm{vv}}(r') \qquad (8)$$

where $h_\alpha^{\mathrm{uv}}(\vec{r})$ is the 3D total correlation function of solvent site γ around the solute macromolecule (the superscripts "u" and "v" denoting the solute and solvent, respectively) giving the normalized deviation of the solvent density from its bulk value, which is related to the 3D solute−solvent site distribution function $g_\gamma(\vec{r}) = h_\gamma(\vec{r}) + 1$, and $c_\alpha^{\mathrm{uv}}(\vec{r})$ is the 3D direct correlation function representing "direct" correlations between the solute and solvent site γ, which has the long-range asymptotics of the 3D solute−solvent site interaction potential: $c_\gamma^{\mathrm{uv}}(\vec{r}) \sim -\beta u_\gamma^{\mathrm{uv}}(\vec{r})$, where $\beta = 1/k_BT$ is the inverse temperature with the Boltzmann constant k_B. The site−site susceptibility of pure solvent $\chi_{\alpha\gamma}^{\mathrm{vv}}(r) = \omega_{\alpha\gamma}^{\mathrm{vv}}(r) + \rho_\alpha^{\mathrm{v}} h_{\alpha\gamma}^{\mathrm{vv}}(r)$ gives the response, in terms of the distributions in pure bulk solvent, of site γ to the presence of site α at separation r. It consists of the intramolecular matrix $\omega_{\alpha\gamma}^{\mathrm{vv}}(r) = \delta(r - l_{\alpha\gamma}^{\mathrm{vv}})/(4\pi(l_{\alpha\gamma}^{\mathrm{vv}})^2)$ specifying the intramolecular correlations of solvent molecules with the geometry given by the **z**-matrix of site separations $l_{\alpha\gamma}^{\mathrm{vv}}$, and the intermolecular part given by the bulk solvent site number density ρ_α^{v} times the site−site radial correlation functions of pure bulk solvent $h_{\alpha\gamma}^{\mathrm{vv}}(r)$. The latter is obtained in advance to the 3D-RISM calculations from the dielectrically consistent RISM theory (DRISM) developed by Perkyns and Pettitt,[49] which provides a consistent description of the dielectric properties for ions in polar solvent. The DRISM integral equation is complemented with the KH closure approximation (see below). The DRISM-KH theory ensures appropriate treatment of systems with strongly associating components, such as aqueous electrolyte solutions and solvent/cosolvent mixtures, in a wide range of concentrations.[6,50−58] While yielding the dielectric properties of polar solvent around the solute macromolecule at the level of a macroscopic dielectric constant, the bulk solvent susceptibility $\chi_{\alpha\gamma}^{\mathrm{vv}}(\vec{r})$ obtained from the DRISM-KH equations and then inserted in the 3D-RISM eq 8 properly accounts for short-range solvation structure effects, such as chemical specificities of solute and solvent molecules, hydrogen bonding, hydrophobicity, steric effects, nanoconfinement, etc.

The convolution in the 3D-RISM eq 8 (as well as that in the DRISM integral equation) is calculated as a product in the reciprocal space. In calculating the forward and backward Fourier transforms between the direct and reciprocal space by using the 3D fast Fourier transform (3D-FFT) technique, the long-range electrostatic parts of the direct and total correlation functions are separated out and handled analytically for both the radial solvent−solvent and 3D solute−solvent correlation functions to ensure their proper asymptotics. For ionic or highly polar solutes, simply truncating the electrostatic asymptotics would lead to catastrophic errors. Using the Ewald summation in a 3D periodic supercell causes huge distortions in the solvation structure and thermodynamics, but the corresponding analytical corrections restore the proper nonperiodic asymptotics of the 3D site correlation functions and accurately eliminate the errors in the solvation chemical potential.[6,59,60] Here we use a somewhat different, nonperiodic version of the analytical account for the electrostatic asymptotics that we had implemented in the 3D-RISM-KH coupled with KS-DFT in the ADF program package.[71] The 3D solute−solvent site interaction potential $u_\gamma^{\mathrm{uv}}(\vec{r})$ and the 3D site correlation functions c_γ^{uv} and h_γ^{uv} are specified on a 3D linear grid in a nonperiodic rectangular box. The electrostatic asymptotics are specified analytically and subtracted from c_γ^{uv} and h_γ^{uv} before applying the 3D-FFT to the remaining short-range parts and then added back after the transform. The 3D box has to be large enough to to have the short-range parts of the 3D site correlation functions around the macromolecular solute decay at its boundaries. It has to be padded with zeros to double size in each dimension when performing the 3D-FFT to prevent aliasing, but can be truncated back to the original size in the direct space after calculating the product $c_\gamma^{\mathrm{uv}}(\vec{r})\chi_{\alpha\gamma}^{\mathrm{vv}}(k)$ for the convolution in eq 8 and performing the backward 3D-FFT. The electrostatic asymptotics of the 3D direct correlation function is given by that of the 3D interaction potential, $c_\gamma^{\mathrm{uv(as)}}(\vec{r}) = -\beta u_\gamma^{\mathrm{uv(as)}}(\vec{r})$. (The asymptotics $c_\gamma^{\mathrm{uv(as)}}(\vec{r})$ and $u_\gamma^{\mathrm{uv(as)}}(\vec{r})$ cancel out in the closure relation (eq 12), see below, and the equations are in fact being solved for the short-range part of $c_\gamma^{\mathrm{uv}}(\vec{r})$.) It is chosen as the potential of the site charges gauss-smeared with half-width η, which has a convenient form in both the direct and reciprocal space (with the suppressed singularity at $r \to 0$ and Gaussian decay for large k),

$$c_\gamma^{uv(as)}(\vec{r}) = -\beta \sum_i \frac{\tilde{Q}_i^u q_\gamma^v}{|\vec{r} - \vec{R}_i|} \operatorname{erf}\left(\frac{|\vec{r} - \vec{R}_i|}{\eta}\right) \quad (9)$$

$$c_\gamma^{uv(as)}(\vec{k}) = -\beta \sum_i \frac{4\pi \tilde{Q}_i^u q_\gamma^v}{k^2} \exp\left(-\frac{1}{4}k^2\eta^2 + i\vec{k}\cdot\vec{R}_i\right) \quad (10)$$

where $\tilde{Q}_i^u$ are point-like partial site charges representing the charge distribution of both the solute electrons and atomic cores, and the smearing parameter is set as $\eta \approx 1$ Å to ensure smoothness of the form of eq 9 within a molecular core and quick decay of the form of eq 10 with k. Substitution of the long-range $c_\gamma^{uv(as)}(\vec{k})$ given by eq 10 into the 3D-RISM integral eq 8 yields the renormalized, long-range $\tilde{h}_\gamma^{uv(as)}(\vec{k}) = \sum_\alpha c_\alpha^{uv(as)}(\vec{k})\chi_{\alpha\gamma}^{vv}(k)$, which has an involved form rather not amenable to analytical transformation to the direct space. However, it suffices instead to introduce a simple analytical form but with the same asymptotic behavior. The electrostatic asymptotics of the 3D total correlation function h_γ^{uv} represents the distribution of solvent site charges resulting in dielectric screening of the solute charge density by solvent polar molecules and Debye screening by solvent ions. Thus, it is dipole−dipole for a polar solute in polar solvent, ion−dipole for an ionic solute in polar solvent, and Debye-screened ion−ion for an ionic solute in electrolyte solution. The latter cannot be neglected in the case of electrolyte solution at medium and especially low ionic concentration, and the analytical electrostatic asymptotics subtracted from h_γ^{uv} before applying the backward 3D-FFT and then added back are thus specified as

$$h_j^{uv(as)}(\vec{k}) = -\beta \sum_i \frac{4\pi \tilde{Q}_i^u q_j^v}{\varepsilon\left(k^2 + \kappa_D^2\right)} \exp\left(-\frac{1}{4}k^2\eta^2 + i\vec{k}\cdot\vec{R}_i\right) \quad (11)$$

$$h_j^{uv(as)}(\vec{r}) = -\beta \sum_i \frac{\tilde{Q}_i^u q_j^v}{\varepsilon|\vec{r} - \vec{R}_i|} \exp\left(-\frac{1}{4}\kappa_D^2\eta^2\right) \times \frac{1}{2}\left\{\exp(-\kappa_D|\vec{r} - \vec{R}_i|)\left[1 - \operatorname{erf}\left(\frac{\kappa_D\eta}{2} - \frac{|\vec{r} - \vec{R}_i|}{\eta}\right)\right] - \exp(\kappa_D|\vec{r} - \vec{R}_i|)\left[1 - \operatorname{erf}\left(\frac{\kappa_D\eta}{2} + \frac{|\vec{r} - \vec{R}_i|}{\eta}\right)\right]\right\} \quad (12)$$

where ε in the dielectric constant of the polar solvent (specified as an input parameter into the DRISM theory for bulk solvent), and $\kappa_D = (4\pi\beta_j\rho_j^v q_j^v 2/\varepsilon)^{1/2}$ is the inverse Debye length of the electrolyte solution with ionic species j of concentrations ρ_j^v.

The 3D-RISM integral eq 8 must be complemented with a closure relating the total and direct correlation functions. Although the exact closure to the Ornstein−Zernike (OZ) integral equation of liquid state theory is known, it has the form of an extremely complex nonlocal functional of the total correlation function.[48] Therefore, it is replaced in practice with approximations adequately representing the physics and/or chemistry phenomena occurring in the system, among the most popular being the so-called hypernetted chain (HNC) closure, mean-spherical approximation (MSA), Percus−Yevick (PY) closure, Verlet closure, Martynov-Sarkisov (MS) closure, and others.[48] It is not trivial difficulty to represent, with just one of these approximations, both short-range features of solvation structure (such as steric effects and excluded volume of the repulsive cores) and long-range effects (association due to chemical specificities in complex liquids and long-range fluctuations in near-critical fluids and liquid mixtures near separation lines). To overcome such difficulties, a renormalization approach was developed in which the interaction potential between the particles is subdivided into a "reference" subsystem amenable to an accurate treatment with one of the closures (for example, liquid of hard-sphere or specially defined repulsive cores) and "the rest" of the interaction potential, typically the long-range part of Lennard−Jones and the electrostatics, and the OZ integral equation is rewritten accordingly. The resulting combined closure provides a considerable improvement, for example, the reference HNC closure (RHNC)[48] very accurately describes a system of Lennard−Jones particles. However, a problem occurs for a strong crossover between short- and long-range features of the solvation structure: repulsive core exclusion areas, association peaks at different distances, and long-range attraction tails of the distribution functions; unfortunately, this is typically the case for complex liquids and liquid mixtures, and a huge variety of macromolecules and nanostructures in solution.

The closures to the RISM and 3D-RISM integral equations for the site−site and 3D site correlations are constructed in analogy with the above closure approximations to the OZ integral equation for simple liquids. The RISM-PY theory pioneered by Chandler and Andersen[61] was successful in describing hard-body molecular fluids. Hirata and co-workers extended the description to polar molecular liquids and electrolyte solutions by proposing the RISM-HNC theory.[62−64] The 3D-RISM-HNC theory was conceptually sketched by Chandler and co-workers in their derivation of density functional theory for classical site distributions of molecular liquids[65,66] and then introduced in that way by Beglov and Roux for polar liquids.[67] Kovalenko and Hirata derived the 3D-RISM integral equation from the six-dimensional molecular Ornstein−Zernike integral equation[48] for the solute−solvent correlation functions by averaging out the orientation degrees of freedom of solvent molecules while keeping the orientation of the solute macromolecule described at the three-dimensional level.[6,47]

The 3D analogue of the so-called hypernetted chain (HNC) closure to the 3D-RISM eq 8 is constructed as

$$g_\gamma^{uv}(\vec{r}) = \exp(-\beta u_\gamma^{uv}(\vec{r}) + h_\gamma^{uv}(\vec{r}) - c_\gamma^{uv}(\vec{r})) \quad (13)$$

where $u_\gamma^{uv}(\vec{r})$ is the 3D interaction potential between solvent site γ and the whole solute. Beglov and Roux[67] have obtained the 3D-RISM/HNC equations, eqs 8 and 13, within the density functional method by reduction of the generalized closure of Chandler, McCoy, and Singer for nonuniform polyatomic systems.[68] In the case of a relatively strong attractive potential between the solute and solvent sites, the 3D-HNC closure 11 can become divergent.[6,47,59,60]

A closure approximation appropriate and successful for the description of the solvation structure and thermodynamics of various inorganic and organic solutes and macromolecules with multiple partial charges in different nonpolar and polar liquids, mixtures, and electrolyte solutions, as well as solid−liquid interfaces has been proposed by Kovalenko and Hirata (KH approximation):[6,47]

$$g_\gamma^{uv}(\vec{r}) = \begin{cases} \exp(X_\gamma^{uv}(\vec{r})) & \text{for } X_\gamma^{uv}(\vec{r}) \le 0 \\ 1 + X_\gamma^{uv}(\vec{r}) & \text{for } X_\gamma^{uv}(\vec{r}) > 0 \end{cases} \quad (14)$$
$$X_\gamma^{uv}(\vec{r}) = -\beta u_\gamma^{uv}(\vec{r}) + h_\gamma^{uv}(\vec{r}) - c_\gamma^{uv}(\vec{r})$$

Equation 14 combines the exponential HNC approximation for the regions of depletion of the distribution function, $g_\gamma^{uv}(\vec{r}) < 1$, the mean spherical approximation (MSA) for the regions of enrichment, $g_\gamma^{uv}(\vec{r}) > 1$, with the function and its first derivative continuous at the joint point $X_\gamma^{uv}(\vec{r}) = 0$. The 3D-KH approximation 12 enforces the proper long-range asymptotics of the direct correlation function $c_\gamma^{uv}(\vec{r})$ in the same way as the original HNC and MSA closures. The MSA-type linearization prevents the artifact of the distribution function diverging in the regions with a large potential. This partial linearization somewhat reduces and widens high peaks of the distribution functions, whereas it much less affects the coordination numbers of the solvation shells.

The 3D-HNC approximation 13 leads to the excess chemical potential of solvation in the closed analytical form[6,47]

$$\Delta\mu^{HNC} = k_B T \sum_\gamma \rho_\gamma^v \int d\vec{r} \left[\frac{1}{2}(h_\gamma^{uv}(\vec{r}))^2 - \frac{1}{2} h_\gamma^{uv}(\vec{r}) c_\gamma^{uv}(\vec{r}) - c_\gamma^{uv}(\vec{r}) \right] \quad (15)$$

equivalent to that derived by Singer and Chandler for the site−site RISM/HNC equations.[69] For the 3D-KH closure 12, the analytical expression is somewhat different,[6,47]

$$\Delta\mu^{KH} = k_B T \sum_\gamma \rho_\gamma^v \int d\vec{r} \left[\frac{1}{2}(h_\gamma^{uv}(\vec{r}))^2 \Theta(-h_\gamma^{uv}(\vec{r})) - \frac{1}{2} h_\gamma^{uv}(\vec{r}) c_\gamma^{uv}(\vec{r}) - c_\gamma^{uv}(\vec{r}) \right] \quad (16)$$

where Θ in the Heaviside step function that puts the term h^2 in effect in the regions of density depletion only.

Accurate calculation of the integral in the excess chemical potential of solvation (14) (or equally in eq 15) requires analytical treatment of the asymptotics of the 3D correlation functions 9 and 12. In the last term in the expression 16, the electrostatic asymptotics of $c_\gamma^{uv}(\vec{r})$ cancel out upon the summation over the site index γ because of the electroneutrality condition. With the short-range parts of the 3D correlation functions decaying at the 3D box boundaries, the asymptotic forms of the first two terms in eq 16 are subtracted from it and then added back, forming the short-range and long-range integrands, with the former integrated numerically over the 3D box volume V and the latter containing just the analytical asymptotics integrated over the whole space,

$$\Delta\mu^{KH} = k_B T \sum_\gamma \rho_\gamma^v \int_V d\vec{r} \left[\frac{1}{2}(h_\gamma^{uv}(\vec{r}))^2 \Theta(-h_\gamma^{uv}(\vec{r})) - \frac{1}{2} h_\gamma^{uv}(\vec{r}) c_\gamma^{uv}(\vec{r}) - c_\gamma^{uv}(\vec{r}) - \frac{1}{2}(h_\gamma^{uv(as)}(\vec{r}))^2 \Theta(Q^u q_j^v) + \frac{1}{2} h_\gamma^{uv(as)}(\vec{r}) c_\gamma^{uv(as)}(\vec{r}) \right] + k_B T \sum_\gamma \rho_\gamma^v \int d\vec{r} \times \left[\frac{1}{2}(h_\gamma^{uv(as)}(\vec{r}))^2 \Theta(Q^u q_j^v) - \frac{1}{2} h_\gamma^{uv(as)}(\vec{r}) c_\gamma^{uv(as)}(\vec{r}) \right] \quad (17)$$

where $Q^u = \sum_i Q_i^u$ is the total charge of the solute, and $q_j^v = \sum_{\gamma \in j} q_\gamma^v$ is the total charge of solute ionic species j which site γ belongs to. The factor $\Theta(Q^u q_j^v)$ switches the asymptotics term $(h_\gamma^{uv(as)}(\vec{r}))^2$ on for like charges of the solute and solvent ion Q^u and q_j^v, and off for unlike ones, according to the term $(h_\gamma^{uv(as)}(\vec{r}))^2 \Theta(-h_\gamma^{uv}(\vec{r}))$ being switched on at long range in the excess chemical potential (16) by the depleted long-range tale of $h_\gamma^{uv}(\vec{r})$ for like charges and off by its enhanced long-range tale for unlike charges. The factor $\Theta(Q^u q_j^v)$ is dropped for the excess chemical potential (15) in the 3D-HNC approximation (13). In the expression (17), the latter integral of the asymptotics over the whole space is analytically reduced to 1D integrals easy to compute,

$$k_B T \sum_\gamma \rho_\gamma^v \int d\vec{r} \left[\frac{1}{2}(h_\gamma^{uv(as)}(\vec{r}))^2 \Theta(Q^u q_j^v) - \frac{1}{2} h_\gamma^{uv(as)}(\vec{r}) c_\gamma^{uv(as)}(\vec{r}) \right] = \frac{1}{\pi} \sum_{\gamma \in v} \frac{\kappa_\gamma^2}{\kappa_D} \int_0^1 dx \sum_{ii' \in u} Q_i^u Q_{i'}^u J_0(\kappa_D l_{ii'}^{uu} x) \times \exp\left(-\frac{1}{2}(\kappa_D \eta x)^2\right) \times \left[\frac{x^2}{\varepsilon(x^2 + (1-x)^2)^2} - \frac{1}{x^2 + (1-x)^2} \right] \quad (18)$$

where $\kappa_\gamma^2 = 4\pi\beta\rho_\gamma^v q_\gamma^v q_j^v/\varepsilon$ is the partial contribution of site γ of solution ionic species j to the Debye length squared, $J_0(x)$ is the zero-order Bessel function of the first kind, and $l_{ii'}^{uu}$ are the site separations between the solute point-like partial site charges $\tilde{Q}_i^u$.

2.3. Self-Consistent Combination of the Orbital-Free Embedding Potential and the 3D-RISM-KH Site Distributions. The principal goal of the present work is the calculation the average solvent dependent shifts in the absorption spectra. To this end, we construct the embedding potential defined in eq 1, which is determined by the averaged electron density of the solvent and use eq 7 to derive the solvent-induced spectroscopic shifts. The 3D-RISM-KH site distributions cannot be directly used to evaluate the orbital-free embedding potential, as they represent not the electron densities needed in eq 1 but the classical nuclear probabilities. To combine the 3D-RISM-KH method with orbital-free embedding framework, two issues must be, therefore, resolved: (i) the procedure to "dress up" the site densities with electrons and (ii) the method to take into account the solute−solvent interactions in generating the classical 3D-RISM-KH site distributions.

2.3.1. Dressing up Classical Site Distributions in Electron Density. The 3D-RISM-KH method is used to obtain the equilibrium density distributions of their classical interaction sites γ. Such distributions do not suffice to evaluate the orbital-free embedding potential as they are essentially related to nuclei and not electrons. The second key new approximation introduced in this work, besides that in eq 7, is the applied procedure to dress up the site distributions with electrons.

First of all, it is assumed that the electron density attributed to each site ($q_\gamma^v(\vec{r})$) is "rigid". This assumption was used already in the first application of the orbital-free embedding potential in simulating solvated system,[34] where it was assumed that a rigid electron density cloud moves together with the nuclei. In other words, the inhomogeneous average electron density of solvent around the solute molecule is obtained as the convolution of the inhomogeneous probability density of the solvent nuclei and the electron density around each of them. Note that the electron density around each nucleus is assumed to be translationally and rotationally invariant. Therefore, inhomogeneities of the average solvent charge density arise due to inhomogeneities of the nuclear distributions. Such construction of $\langle \rho_B(\vec{r}) \rangle$ neglects, therefore, any instantaneous fluctuations of the electron density of each solvent molecule due to fluctuations of its induced dipole moments. Note, however, that the rigid density

used for each solvent molecule does not correspond to the gas phase but to the liquid. The averaged electron density of the solvent is obtained thus as:

$$\langle \rho_B(\vec{r}) \rangle = \sum_\gamma \int \mathrm{d}\vec{r}\,' q_\gamma^{\mathrm{v}}(|\vec{r} - \vec{r}\,'|) \rho_\gamma^{\mathrm{v}} g_\gamma^{\mathrm{uv}}(\vec{r}\,') \qquad (19)$$

where the angle brackets $\langle ... \rangle$ denote the statistical ensemble average, and $g_\gamma^{\mathrm{uv}}(\vec{r})$ is the 3D solute−solvent site distribution function obtained from the 3D-RISM-KH theory described in the previous section.

Such simplified construction of the electron density of the environment was used in a number of our subsequent applications in liquids.[28,29] In the present work, a further simplification is introduced: the rigid electron densities are orientationally averaged, spherically symmetric distributions centered at atoms (O and H in the case of water, for instance) or groups of atoms (O, H, and CH_3, in the case of methanol, for instance). The third approximation made in the procedure to dress-up the RISM site distributions concerns the evaluation of the convolution (eq 19). We note that the functions $q_\gamma^{\mathrm{v}}(\vec{r})$ are short ranged whereas the RISM grid at which the site distributions are evaluated is large (0.5 Å). Therefore, to a good approximation, the integration can be replaced by summation involving only diagonal elements, with the weights corresponding to the number of electrons associated to each site (8.8 e for oxygen in water and 0.6 e for a hydrogen in water for instance). This assumption means that the weights represent the average charge distribution in the solvent molecule, which is not affected by the instantaneous configuration of the solvent. Lifting this simplification by using an orientation-dependent charge density $q_\gamma^{\mathrm{v}}(r, \Omega)$ would involve the orientation-dependent site distributions $g_\gamma^{\mathrm{uv}}(\vec{r}, \Omega)$. As a consequence, solving 3D-RISM equations would become significantly more involved. It is important to underline that the average charge distribution differs, however, from its gas-phase counterpart.

The three above assumptions lead to the following expression for $\langle \rho_B(\vec{r}) \rangle$ at the 3D-RISM grid, which reads:

$$\langle \rho_B(\vec{r}) \rangle = \sum_\gamma q_\gamma^{\mathrm{v}} \rho_\gamma^{\mathrm{v}} g_\gamma^{\mathrm{uv}}(\vec{r}) \qquad (20)$$

2.3.2. Solute−Solvent Interactions in the 3D-RISM-KH Approach. To account for the solute−solvent coupling in the 3D-RISM-KH calculations aimed at obtaining the site distributions g^{uv}, we adopt the same approach as the one introduced in our previous work on embedding a Kohn−Sham system in the average solvent potential generated by the 3D-RISM-KH method.[71,72] Here, the solute−solvent coupling is represented in a classical way. Its basic features are outlined below.

The use of the average electron density of the solvent, that is, $\langle \rho_B(\vec{r}) \rangle$ in eq 4, is based on the generalization of the Hohenberg−Kohn energy functional to the ensembles of solvent conformations. This can be made similarly to the case of density functional theory for ensembles of electronic states in which ensemble operators and mean values for the system quantities are defined.[74,75] The whole system is thus described by means of the Helmholtz free energy functional

$$\langle A \rangle [\langle \rho_A \rangle, \{\rho_\gamma^{\mathrm{v}}\}] = \langle E_{\mathrm{A}} \rangle [\langle \rho_{\mathrm{A}} \rangle, \langle \rho_{\mathrm{B}} \rangle] + \Delta\mu_{\mathrm{solv}}^{\mathrm{KH}}[\{\rho_\gamma^{\mathrm{v}}\}] \qquad (21)$$

of the mean electronic density of the embedded molecule $\langle \rho_{\mathrm{A}}(\vec{r}) \rangle$ and the set of the classical 3D solvent site density distributions $\rho_\gamma^{\mathrm{v}}(\vec{r}) = \rho_\gamma^{\mathrm{v}} g_\gamma^{\mathrm{uv}}(\vec{r})$ for all solvent sites γ. At this stage, assuming the coupling between the embedded subsystem A and environment B to be weak enough we apply the same above-described OFE functionals to the mean densities $\langle \rho_{\mathrm{A}}(\vec{r}) \rangle$ and $\langle \rho_{\mathrm{B}}(\vec{r}) \rangle$. For simplicity, we will drop the ensemble averaging brackets in all notations below, keeping in mind that all quantities are mean values averaged over the ensemble of the environment.

The environment electron density obtained from the 3D-RISM theory in the form 20 can be used right away to calculate the nonelectrostatic components $v_{\mathrm{xc}}^{\mathrm{nad}}[\rho_{\mathrm{A}}, \rho_{\mathrm{B}}](\vec{r})$ and $v_t^{\mathrm{nad}}[\rho_{\mathrm{A}}, \rho_{\mathrm{B}}](\vec{r})$ of the embedding potential $v_{\mathrm{emb}}^{\mathrm{KSCED}}[\rho_{\mathrm{A}}, \rho_{\mathrm{B}}; \vec{r}]$ defined in eq 1. Furthermore, the electrostatic terms in the embedding potential $v_{\mathrm{emb}}^{\mathrm{KSCED}}[\rho_{\mathrm{A}}, \rho_{\mathrm{B}}; \vec{r}]$, explicitly dependent on the positions of the environment nuclei in the original OFE, are replaced in our ensemble approach by the statistical-mechanical average of the electrostatic potential of solvent sites acting on the solute, defined as a variational derivative of the system free energy 19 with respect to the embedded density $\rho_{\mathrm{A}}(\vec{r})$:

$$v_{\mathrm{solv}}^{\mathrm{elec}}(\vec{r}) \equiv \frac{\mathrm{A}[\rho_{\mathrm{A}}, \{\rho_\gamma^{\mathrm{v}}\}]}{\delta\rho_{\mathrm{A}}(\vec{r})} = \sum_\gamma \rho_\gamma^{\mathrm{v}} \int \mathrm{d}\vec{r}\,' v_\gamma^{\mathrm{el}}(|\vec{r} - \vec{r}\,'|) h_\gamma^{\mathrm{uv}}(\vec{r}\,') \qquad (22)$$

where $v_\gamma^{\mathrm{el}}(\vec{r})$ is the electrostatic potential created by the site electronic charge density $q_\gamma^{\mathrm{v}}(\vec{r})$, and $h_\gamma^{\mathrm{uv}}(\vec{r}) = g_\gamma^{\mathrm{uv}}(\vec{r}) - 1$ is the 3D solute−solvent site total correlation function obtained from the 3D-RISM-KH theory. Note that the expression 22 is obtained by definition with the variational differentiation of the expression for the solvation chemical potential of the embedded molecule with respect to its electronic density $\rho_{\mathrm{A}}(\vec{r})$.[47]

The 3D-RISM-KH integral eqs 8 and 14 are solved for the 3D solute−solvent site correlation functions describing the classical solvation structure around the embedded solute molecule, using the input of the classical interaction potentials $u_\gamma^{\mathrm{uv}}(\vec{r})$ of the solute acting on solvent site γ that enter the closure relation 14. In a self-consistent field loop, these interaction potentials are defined by the variational differentiation of the system free energy functional 21 with respect to the classical 3D solvent site density distributions $\rho_\gamma^{\mathrm{v}}(\vec{r})$. We further break them up into the short-range interaction part represented by the sum of the Lennard−Jones potentials $u_{i\gamma}^{\mathrm{uv(LJ)}}(\vec{r})$ between solvent site γ and all the atoms i centered at positions $\vec{R}_i$ in the embedded solute molecule, the electrostatic interaction potential between the solvent site charge density $q_\gamma^{\mathrm{v}}(\vec{r})$ and the solute atomic cores with charges Q_i^{u} at $\vec{R}_i$, and the electrostatic interaction potential between the solvent site and the valence electron density of the embedded molecule $\rho_{\mathrm{A}}(\vec{r})$,[47,71]

$$u_\gamma^{\mathrm{uv}}(\vec{r}) \equiv \frac{A[\rho_{\mathrm{A}}, \{\rho_\gamma^{\mathrm{v}}\}]}{\delta\rho_\gamma^{\mathrm{v}}(\vec{r})} = \sum_i \left(u_{i\gamma}^{\mathrm{uv(LJ)}}(|\vec{r} - \vec{R}_i|) + \int \mathrm{d}\vec{r}\,' \frac{Q_i^{\mathrm{u}} q_\gamma^{\mathrm{v}}(|\vec{r}\,' - \vec{r}|)}{|\vec{r} - \vec{R}_i|} \right) - \mathrm{e} \int \mathrm{d}\vec{r}\,' \mathrm{d}\vec{r}\,'' \frac{\rho_{\mathrm{A}}(\vec{r}\,') q_\gamma^{\mathrm{v}}(|\vec{r}\,'' - \vec{r}|))}{|\vec{r}\,'' - \vec{r}\,'|} \qquad (23)$$

The latter term in eq 23 is calculated in the density fitting procedure.[76] Following the standard force fields, the solvent site charge densities $q_\gamma^{\mathrm{v}}(\vec{r})$ can be represented with point-like partial charges q_γ^{v} to simplify this expression to

$$u_{\gamma}^{uv}(\vec{r}) = \sum_{i}\left(u_{i\gamma}^{uv(LJ)}(|\vec{r} - \vec{R}_i|) + \frac{Q_i^u q_\gamma^v}{|\vec{r} - \vec{R}_i|}\right) - e\int d\vec{r}\,'\frac{\rho_A(\vec{r}\,')q_\gamma^v}{|\vec{r}\,' - \vec{r}|} \quad (24)$$

Note that the analytical form for the free energy of solvation (eq 16) and for the coupling potentials (eqs 22 and 23) yield the analytical expressions for the derivatives of the system free energy (eq 21) with respect to nuclei coordinates R_i of the embedded molecule. As a consequence, efficient algorithms based on analytic gradients can be used in the geometry optimization and reaction pathway studies of solvated systems.[71,72]

Practical applications of eq 4 involve numerical integration on the grid. The adequate grid used for this purpose extends on both the embedded system and its environment and, similarly to grids used in solving the Kohn−Sham equations, is not uniform. The 3D-RISM-KH calculations use also a grid which is, however, different. The classical site distributions are more homogeneous than the electron density. To facilitate evaluation of the Fourier transforms, it is uniform and cubic. Calculations, which involve the combination of these two grids, are implemented in our local version of the ADF 2008 program[76,77] and involve four principal stages: (i) The OFE module is used to generate the OFE grid. (ii) The 3D-RISM-KH site distributions are evaluated on the 3D-RISM grid and dressed up with electrons. The density $\langle\rho_B(\vec{r})\rangle$ and the corresponding electrostatic potential are thus evaluated on the 3D-RISM grid. The numerical values of these quantities are interpolated on the OFE grid (obtained in stage (i)) and imported into the 3D-RISM module. (iii) The interpolated density and potential are imported back to OFE module,[19] which solves eq 4, and obtains all the quantities needed to evaluate the excitation energies following the approach introduced in ref 40, that is, embedded orbitals, their energies, and the contribution to the response kernel due to the orbital-free embedding potential. (iv) Evaluation of the excitation energies. The modification of the ADF 2008 code allowing for such calculations concern primarily the stage (ii), which involves dressing up the classical site distributions with electrons and interfacing the grid generated at stage (i) with that needed at stage ii. Concerning the solver of eq 4 and the solver of LR-TDDFT response equations for embedded system the numerical implementation of the methodology introduced in the present work do not require any specific code modifications.

Finally, we point out that difference between the approach taken in the present work and that in refs 71 and 72 lies in the embedding potential used in quantum mechanical part of the applied computational protocol and not in the evaluation of the classical site distributions which are evaluated in the same way as in refs 71 and 72. Compared to the embedding potential of Wesolowski and Warshel[12] (eq 1), the embedding potential used in the previous studies comprises only the first two electrostatic terms of $v_{emb}^{KSCED}[\rho_A, \rho_B; \vec{r}]$. Such simplification corresponds to a purely electrostatic embedding. The neglected terms $v_{xc}^{nad}[\rho_A, \rho_B](\vec{r})$ and $v_t^{nad}[\rho_A, \rho_B](\vec{r})$, which account for the Pauli repulsion, were shown to be indispensable in many types of embedded systems.[30,40,73]

3. Computational details

3.1. 3D-RISM-KH. To obtain the solvent site distributions and atomic charges of the solvent which are self-consistent, the Kohn−Sham DFT/3D-RISM-KH scheme introduced and recently implemented by Gusarov et al.[71] in the ADF program package[76] was used. The size of the 3D-FFT grid was chosen to be 64 × 64 × 64 points in cell size 32 × 32 × 32 Å (64 × 64 × 128 in cell size 32 × 32 × 64 Å for benzophenone). In the KS-DFT/3D-RISM-KH scheme the partial charges used for the solute are taken from the multipole-derived population analysis (labeled as mdc-q in ADF output).[78] To ensure the high quality of these charges, STO(TZP) basis set with modified fit functions to give better multipole moments was used.[78] For the exchange-correlation functional LDA approximation[79−81] was used, integration parameter was set to 6.0. The van der Waals parameters required to solve 3D-RISM-KH equations were taken from OPLS force field.[82,83] If not stated otherwise, in all calculations the geometry of considered chromophores was optimized in gas-phase in KS-DFT framework using BP86 exchange-correlation functional.[84,85]

3.2. Orbital-Free Embedding. The effective embedding potential given in eq 1 is evaluated for each instantaneous pair of densities, $\rho_A(\vec{r})$ and $\langle\rho_B(\vec{r})\rangle$, using the following approximants:

(1) For the $v_t^{nad}[\rho_A, \rho_B](\vec{r})$ component of the embedding potential, its analytic form was obtained using eq 2 applied to the Thomas-Fermi expression for kinetic energy functional.[86,87]

(2) For the $v_{xc}^{nad}[\rho_A, \rho_B](\vec{r})$ component of the embedding potential, local density approximation was used for its exchange[79] and correlation parts.[80,81]

The electrostatic component was evaluated using the monomer expansion of the 3D-RISM potential using all the centers of the 3D-RISM grid (see eq 22).

The exchange-correlation component of the total effective potential in eq 4, which is generated by the embedded density ρ_A, i.e., $(\delta E_{xc}[\rho_A])/(\delta\rho_A)$, is approximated using the SAOP potential.[88,89] Such hybrid treatment of the total exchange-correlation potential is motivated by the fact that SAOP is known to describe better the electronic excitations in the isolated chromophore. Note that SAOP cannot be used for approximating the corresponding component of the orbital-free embedding potential because it depends explicitly on orbitals which are not available for $\rho_A + \rho_B$.

In all calculations, the orbitals of the chromophore are expanded using the Slater type of atomic orbitals (TZ2P basis set), which included only atomic centers localized in the chromophore (the (KSCED(m) variant of the finite basis version of eq 4[90]). The integration parameter for the grid generation was set to 6.0.

4. Results and Discussion

For the following chromophores: aminocoumarin C151, acetone, acrolein, and benzophenone, the solvatochromic shifts are discussed in separate sections below. The lowest lying excitations of the $\pi \rightarrow \pi^*$ and/or $n \rightarrow \pi^*$ type are discussed. The solvatchromism of acetone and amnocoumarin in water was already studied using the orbital-free embedding strategy.[28,29] The previous simulations did not use the key approximation introduced in the present work, given in eq 7, and can be used as the reference for establishing adequacy of this approximation.

The analysis of the significance of the nonelectrostatic components of the embedding potential is provided in the separate section.

4.1. Aminocoumarin C151. We start the analysis of the solvatochromic shifts for the $\pi \rightarrow \pi^*$ excitations in aminocoumarin C151 (see Figure 1). Experimental[91−93] as well as theoretical studies[95,96] including previous work applying the embedding potential of eq 1[29] indicate that the lowest absorption band is of the $\pi \rightarrow \pi^*$ character showing pronounced red-shift in polar solvents.

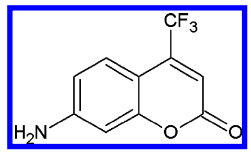

Figure 1. Structure of aminocoumarin C151.

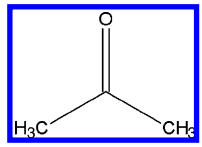

Figure 2. Structure of acetone.

TABLE 1: Solvatochromic Shifts from Water to Gas Phase of Aminocoumarin $\pi \rightarrow \pi^*$ Absorption Band Calculated Using Orbital-Free Effective Embedding Potential and the Two Strategies to Account for the Statistical Nature of the Solvent: Explicit and Thorough 3D-RISM[a]

model of solvent	$\Delta\varepsilon$ [eV]
explicit: 300 H_2O, 50 snapshots (ref 29)	−0.28
explicit: 300 H_2O, 400 snapshots (ref 29)	−0.25
3D-RISM	−0.25
experiment	−0.22[b]

[a] Data taken from Neugebauer et al.[29] For description see text. [b] Reference 91.

Aminocoumarin C151 is especially suited for the analysis of the key approximation in the computational approach introduced in eq 7 of the present work, that is, the replacement of a large number of calculations spectral shifts for different configurations of the solvent to obtain averages by only one calculation but using the average embedding potential. In simulations reported in ref 29 as well as in the present work, the orbital-free embedding potential given in eq 1 was used to obtain the shifts between the absorption maxima in the gas phase and in water. Therefore, the solvatochromic shifts obtained following these two strategies can be used to analyze the adequacy of the approximation made in eq 7.

The spectral shifts were evaluated in ref 29 using either 50 or 400 configurations of 300 solvent molecules. The configurations were taken from either one or eight 50 ps long equilibrated molecular dynamic trajectory. The calculated spectral shifts reported in ref 29 amount to −0.28 and −0.25 eV for the 50 or 400 configuration based statistics, respectively. These values are in remarkable agreement with the OFE/RISM results (see Table 1). This agreement calls for a more detailed analysis. The OFE/RISM results could be considered as the ensemble average only if the orbital-free embedding potential was independent of ρ_A. In such a case, eq 7 would not be an approximation but an exact expression. Our dedicated studies on the dependence of the orbital-free embedding potential on ρ_A showed that indeed this dependence is weak[94] for the type of intermolecular interactions as the ones occurring in the systems studied here. This justifies treating the OFE/RISM shifts as a target and interpreting the agreements between the shifts obtained as averages over 400 ps long MD trajectory and the OFE/RISM results as the evidence that the trajectory obtained in ref 29 adequately represents the statistical ensemble. Note that the OFE/RISM strategy requires only one evaluation of the excitation energies whereas the explicit strategy requires 400 of such evaluations.

The results of the OFE/RISM calculations together with the survey of available experimental data are gathered in Table 2. In this table (and in respective tables for other examples considered in the present work), the values in parentheses are obtained using the electrostatic-only embedding, that is, with the $v_{xc}^{nad}[\rho_A, \rho_B](\vec{r})$ and $v_t^{nad}[\rho_A, \rho_B](\vec{r})$ terms in eq 1 neglected. They will be discussed in a separate section of this work.

TABLE 2: Calculated Excitation Energies and Solvatochromic Shifts (in [eV]) to the Gas Phase of $\pi \rightarrow \pi^*$ Absorption Band in Aminocoumarin[a]

solvent	$\varepsilon_{OFE/RISM}$	$\Delta\varepsilon_{OFE/RISM}$	$\Delta\varepsilon_{exp}$[b]
H_2O	2.988 (2.985)	−0.25 (−0.25)	−0.22
methanol	3.028 (3.029)	−0.21 (−0.21)	−0.31
diethyl ether	3.102 (3.103)	−0.13 (−0.13)	−0.21
n-hexane	3.236 (3.235)	0.00 (0.00)	
gas phase	3.234		

[a] The numbers in parentheses correspond to the case when electrostatic-only embedding is used. [b] Reference 91.

TABLE 3: Excitation Energies and Solvatochromic Shifts to the Gas-Phase of $\pi \rightarrow \pi^*$ Absorption Band in Aminocoumarin Calculated with the COSMO model (Excitation Energies and Shifts in [eV])

solvent	ε_{COSMO}	$\Delta\varepsilon_{COSMO}$	$\Delta\varepsilon_{exp}$[a]
H_2O	3.041	−0.19	−0.22
methanol	3.043	−0.19	−0.31
diethyl ether	3.089	−0.14	−0.21
n-hexane	3.157	−0.08	
gas phase	3.234		

[a] Reference 91.

In all of considered solvents, the calculated lowest-lying excitations have the $\pi \rightarrow \pi^*$ character, are red-shifted compared to the free chromophore, and agree reasonably well with experiment. For water, OFE/RISM overestimates the solvatochromic shift by only 0.03 eV. In the case of the other two considered solvents, 65% (for methanol) and 63% (for dimethyl ether) of the experimental shifts is recovered. Discrepancies between the experimental and calculated shifts can be attributed to several factors. The most probable ones are the errors due to approximants to the density functionals in eq 1, the neglect of dynamic response of the environment, and the treatment of the statistical nature of the solvent. The agreement between the shifts obtained for aminocoumarin in water in the present work with the previously published data[29] suggest that the last factor is less important. The analyses of ref 29 also indicate that NDRE is most likely the main contributor to the error.

The widely used COSMO model,[97] is based on the continuum representation of the solvent. It is useful to compare the results obtained with the two levels of description of the solvent: COSMO (Table 3) and OFE/RISM (Table 2). Similarly to OFE/RISM, the COSMO shifts are in reasonable agreement with experiment. OFE/RISM is clearly superior for the nonpolar solvent (n-hexane), whereas the two methods lead to very similar results for more polar solvents.

Neither OFE/RISM nor COSMO describe the fact that the magnitude of the solvatomic shift is smaller in water than in methanol. The failure to describe the larger magnitude of the solvatochromic shifts of the $\pi \rightarrow \pi^*$ transition in aminocoumarin in methanol than in water by mean of either methods remains to be clarified.

Considering practical use of discussed here methods, the LR-TDDFT calculations of isolated aminocoumarin take 2.5 h or single core machine, while including solvent by either COSMO or OFE/RISM takes 3 and 7 h, respectively. It can be seen that compared to COSMO, OFE/RISM calculations involve about 2-fold increase in the time of calculations performed using the

TABLE 4: Calculated Excitation Energies and Solvatochromic Shifts (in [eV]) to the Gas Phase of $n \rightarrow \pi^*$ Absorption Band of Acetone[a]

solvent	$\varepsilon_{OFE/RISM}$	$\Delta\varepsilon_{OFE/RISM}$	$\Delta\varepsilon_{exp}$[b]
H_2O	4.768 (4.727)	0.19 (0.15)	0.22, (0.19 − 0.21[c])
methanol	4.702 (4.683)	0.12 (0.10)	0.12, (0.15[d])
diethyl ether	4.638 (4.616)	0.06 (0.04)	0.02, (0.04[e])
n-hexane	4.592 (4.585)	0.01 (0.00)	−0.004[e]
gas phase	4.581		

[a] The numbers in parentheses correspond to the case when electrostatic-only embedding is used. [b] The most recent re-examination of experiment data provided in ref 114 is used as reference. The results of previous experimental studies are given in parentheses. [c] Reference 108−112. [d] Reference 111. [e] Reference 113.

ADF implementation of these two methods. This indicates that introducing a more realistic level of the description of the solvent by replacing the simplest continuum by nonuniform 3D-RISM site probabilities involves acceptable additional CPU costs.

4.2. Acetone. Acetone is commonly used as a model system to test the accuracy of theoretical methods to predict solvatochromic shifts.[28,37,98−107] For the survey and comparison of available computational studies, see ref 37. Acetone is also very well characterized experimentally.[108−112] For the overview of the experimental data, see the recent analyses by Renge.[114] The previous studies, where the orbital-free embedding strategy to calculate the solvatochromic shifts of acetone in water was also applied but the averaging was made without the approximation introduced in eq 7, provide excellent reference.[28]

The experimental studies indicate that the lowest transition in acetone is of the $n \rightarrow \pi^*$ character. The solvatochromic shift in water is well estimated to be between 0.19−0.22 eV.[108−112,114] Our results are gathered in Table 4.

For all of the considered solvents, OFE/RISM predicts the lowest excitation (HOMO to LUMO) to be the $n \rightarrow \pi^*$ transition. The magnitude of the excitation energy increases with the polarity of the solvent. Comparison of solvatochromic shifts with the experimental results reveals good agreement in all of the cases. For nonpolar solvents, such as n-hexane, the calculated shift is very small, which corroborates with the recent experimental reports.[114] In the case of the diethyl ether, the experimental result is slightly overestimated by 0.04 eV. For polar solvents the results are also close to the reference data. For methanol, the OFE/RISM combination predicts shift to be equal to 0.12 eV, which is in remarkable agreement with the most recent experimental studies.[114] In the case of the water, the estimated solvatochromic shift is within the range of the reference values. In summary, the proposed computational approach describes acetone in a proper way.

Recently, Neugebauer et al.[28] applied the orbital-free embedding formalism and explicit solvent level for acetone in water. The instantaneous electron densities of the solvent (about 175 atoms) were calculated for 220 configurations extracted from equilibrated CPMD trajectory and used to evaluate the instantaneous excitation energies. The reported average solvatochromic shift equal to 0.20 eV evaluated in this tedious and laborious protocol requiring considerable amount of computer resources, is in excellent agreement with the shift obtained in the present work. Using 3D-RISM-KH to generate $\langle\rho_B\rangle$ reduces the time of computations to only 25 min and leads to the spectral shift (0.19 eV) also in good agreement with experiment. Owing to the approximation introduced in eq 7, the repetitive generation solvent density for each solvent configurations is avoided. The obtained shifts with- and without the approximation given in eq 7 agree excellently with the most recent experimental data[114] (0.22 eV). Moreover, the most recent theoretical value for this shift obtained using high-level ab initio description (CCSD) of the acetone are also very similar (0.20 eV[37]).

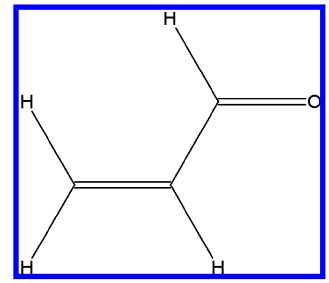

Figure 3. Structure of *s-trans*-Acrolein

In the same work,[28] the authors identify and report the $\sigma - \pi^*$ valence transition, which is not known experimentally due to the low intensity, however, calculations reveal strong red-shift in excitation energy when going from gas-phase to water. For instance, Neugebauer et al. report the shift of −0.32 eV for a single configuration of 57 water molecules taken from equilibrated MD trajectory. The authors do not report, however, the averaged value of this shift, making direct comparisons with our OFE/RISM result (−0.23 eV) impossible. In view of this, both calculated shifts appear consistent.

4.3. Acrolein. *s-trans*-Acrolein (Figure 3) is a simple aldehyde, for which the lowest transition has the $n \rightarrow \pi^*$ character. The absorption spectra are available.[115−126] Most recent measurements estimate that the absorption energy of acrolein solvated in water is blue-shifted by 0.25 eV with respect to gas-phase.[115] The theoretical studies for this spectrum were reported[127−132] (for survey see ref 115). In the work by Tenno,[106] where SCF-RISM method was applied to obtain excitation energies, the authors report the change in the absorption band upon solvation to be 0.20 eV, in good agreement with the experiment. The spectral shift obtained in the present study (0.33 eV) overestimates slightly the experimental result.

4.4. Benzophenone. Benzophenone (see Figure 4) is an interesting molecule for theoretical studies. The experimental UV-vis absorption spectra[133] is characterized by two main bands: the first one of the $n \rightarrow \pi^*$ character, and the second broad one is of the $\pi \rightarrow \pi^*$ type. Experiment also reveals that, upon solvation, the $n \rightarrow \pi^*$ excitation is blue-shifted, whereas the $\pi \rightarrow \pi^*$ band shows pronounced red-shift.

The OFE/RISM solvatochromic shifts in the benzophenone combination are given in Table 5. The geometry of the solute was taken from ref 134. The broad $\pi \rightarrow \pi^*$ band originates from four transitions. The intensity weighted average of the calculated absorption lines is, therefore, used for comparisons with experiment. For methanol and diethyl ether, the OFE/RISM describes very well the both blue- and red-shifts in $n \rightarrow \pi^*$ and $\pi \rightarrow \pi^*$ transitions. The deviation from the experimental findings does not exceed 0.02 eV. For water, the calculated shifts are less satisfactory. The OFE/RISM results recover only 59 and 50% of the experimental shifts, in $n \rightarrow \pi^*$ and $\pi \rightarrow \pi^*$ transitions, respectively. This underestimation might originate from both the interpretation of the experimental data or from the many simplifications/approximations in the computational protocol applied in this work. The experimental studies[133] indicate that with the increasing polarity of the solvent the formation of the shoulders in absorption spectrum is observed. In the case of water, this effect is already pronounced and it leads to the uncertainty in experimental absorption maxima as large as 0.1 eV. Concerning the possible deficiencies in the

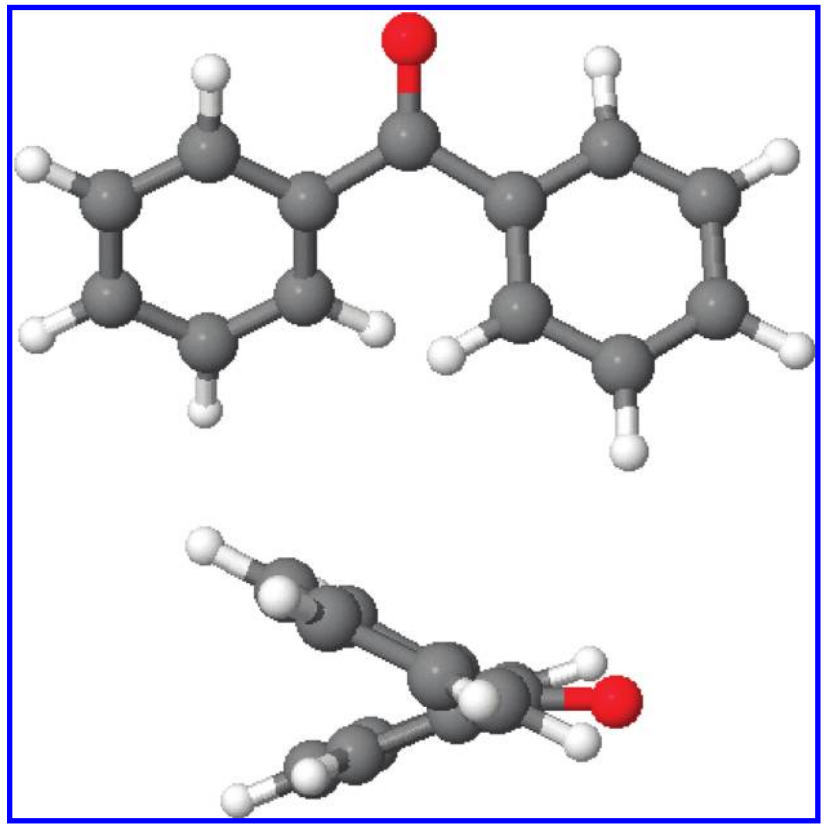

Figure 4. Structure of benzophenone taken from ref 134.

TABLE 5: Solvatochromic Shifts (In [eV]) to the Gas Phase for Benzophenone[a]

solvent	transition	$\Delta\varepsilon_{OFE/RISM}$	$\Delta\varepsilon_{exp}$ [b]
H_2O	$n \rightarrow \pi^*$	0.16 (0.14)	0.27
	$\pi \rightarrow \pi^*$	−0.10 (−0.12)	−0.20
methanol	$n \rightarrow \pi^*$	0.16 (0.16)	0.16
	$\pi \rightarrow \pi^*$	−0.08 (−0.09)	−0.10
diethyl ether	$n \rightarrow \pi^*$	0.06 (0.06)	0.03
	$\pi \rightarrow \pi^*$	−0.02 (−0.02)	−0.03
hexane	$n \rightarrow \pi^*$	0.00 (0.00)	
	$\pi \rightarrow \pi^*$	0.00 (0.00)	

[a] The shift in the $\pi \rightarrow \pi^*$ transition is calculated as the average $\langle\varepsilon\rangle = (\sum_i \varepsilon_i \omega_i)/(\sum_i \omega_i)$, where ε denotes the transition energy and ω the corresponding intensity. The numbers in parentheses correspond to the case when electrostatic-only embedding is used. [b] Reference 133.

calculations reported here, the discrepancy between the experimental and calculated data could be attributed to the underestimated average polarization of the benzophenone molecule by the solvent. The detailed analysis of the simulations reported in ref 134 support such attribution. In the approach applied in ref 134, the induced dipole moment of the solute was obtained in a self-consistent manner to correspond to the structure of the solvent molecules, and the authors stress the importance of proper accounting of this effect in proper modeling of the solvatochromic shifts. It is worth noting that this requirement of self-consistency between the electronic and solvation structures of the solute is met in the present work due to the electrostatic coupling between the solute charges (from quantum mechanical calculations) and the solvent site distributions (from classical statistical-mechanical calculations). The self-consistent solute charges are evaluated taking into account the electrostatic coupling with the solvent. The charges accounting for the electron distribution on the solute are self-consistently recalculated for every new distribution of the solvent sites in the self-consistent field loop. The converged dipole moment of benzophenone solvated in water given by Georg et al. is equal to 5.84 D, which is significantly larger than that of the isolated solute by 2.73 D (MP2/6-311++G(d,p) calculations). In the present work, the corresponding values are 5.89 and 2.16 D, respectively. The solute−solvent interaction-induced increase of the dipole moment of benzophenone is, probably, underestimated in the present OFE/RISM calculations. The interpretation that this underestimation as the principal source of the underestimation of the OFE/RISM solvatochromic shifts in the $n \rightarrow \pi^*$ transition, is supported by the fact that the shift obtained in ref 134 (0.25 eV) is in excellent agreement with experiment (0.27 eV), whereas the OFE/RISM result is significantly underestimated (0.16 eV). Turning back to the possible underestimation of the solvation induced dipole moment of benzophenone in OFE/RISM calculations, it probably results from the basic approximation made in evaluating averages made in this work, that is, eq 7.

4.5. The Role of the Nonelectrostatic Terms in the Orbital-Free Embedding Potential. Various embedding schemes are currently in use for simulations of condensed matter. In view of the studies aimed at the electronic structure, it is worthwhile to underline that it is determined by the way the environment is represented at the level of the electronic Hamiltonian rather than in the final expression used for the energy. According to the exact embedding theory,[12−14] the embedding potential comprises nonelectrostatic terms. Very commonly, only electrostatic potential is used to represent the environment in the Hamiltonian. Moreover, this potential is frequently evaluated not exactly but it is simplified using the multicenter multipole expansion of the electrostatic potential generated by the environment, for instance. Such approach is adequate especially if the target of the simulations is the potential energy surface. The

nonelectrostatic contributions to the total energy are added a posteriori as additional terms in the energy. This approach is know in literature to provide reliable results and is commonly used to treat problems in the fields of chemistry and biochemistry.[136] In studies of the electronic structure, electrostatic embedding leads sometimes to artifacts. It may lead, for instance, to artificial charge transfer from the embedded system to the environment caused by strong Coulomb attraction in the vicinity of solvent nuclei.[18,73,137] The full embedding potential given in eq 1 comprises the nonelectrostatic components in addition to the electrostatic potential. The role of the $v_t^{\mathrm{nad}}[\rho_A, \rho_B](\vec{r})$ component of the embedding potential is to provide counterbalancing repulsive force[73] eliminating such artifacts.

In the present work, the electrostatic potential of environment in eq 1 is obtained from 3D-RISM-KH method as a statistical-mechanical average of the electrostatic potentials of solvent sites acting on embedded system (eq 22). This potential was already used to account for solvent effects in connection with Kohn−Sham method[47,71,72] or with Hartree−Fock[138,106] and multiconfigurational methods.[139] To estimate the role of the nonelectrostatic components in the embedding potential, each of the numerical value discussed in the previous section is complemented by its counterpart obtained with neglecting nonelectrostatic terms in eq 1. The numerical values are given in parentheses in Tables 2, 4, 5. We start the analysis from acetone (Table 4). In the case of this molecule the effect of the nonelectrostatic terms is rather noticeable for polar solvents, especially for water. It increases the magnitude of the solvatochromic shift by 0.04 eV, that is, by 21%. The relative effects decreases with decreasing polarity of the solvent: 16% for methanol and decreases further for diethyl ether and hexane.

In the case of benzophenone (Table 5), the strongest effect of neglecting nonelectrostatic terms occurs for water. The solvatochromic shift is affected by 0.03 eV, that is, 12 and 27% of the whole shift for the $n \rightarrow \pi^*$ and $\pi \rightarrow \pi^*$ transitions, respectively. For other solvents, the electrostatic-only embedding potential seems to be already accurate as it leads to practically the same shifts as the full $v_{\mathrm{emb}}^{\mathrm{KSCED}}[\rho_A, \rho_B; \vec{r}]$ potential.

The solvatochromic shifts in aminocoumarin are not noticeably affected by neglecting nonelectrostatic terms.

The above results indicate that nonelectrostatic terms in the embedding potential affect most significantly the calculated shifts in such cases where the environment constitutes polar molecules with large dipole moment. This result is in line with our previous analyses of the embedding potential of charged systems, for which a significant charge-transfer from embedded molecule to the embedded system can be expected to happen in the absence of two terms in the embedding potential representing the intermolecular Pauli repulsion.[140]

5. Conclusions

In this work, the ensemble average of the charge density of the solvent is used to represent the solvent surrounding a chromophore. Such treatment can be situated between the explicit atomistic- and the continuum-type of models of the solvent. The average charge density accounts for inhomogeneity in the statistically averaged electron density but does not correspond to the electron density of any molecular system at a given geometry. Nevertheless, owing to the unique correspondence between the pair of electron densities (that of the chromophore and of its environment) and the embedding potential,[12−14] the formalism used previously to evaluate spectral shifts in cases where the environment of a chromophore was structurally rigid[22,40] can also be used for cases where the electron density of the environment lacks such a clear interpretation.

The averaged electron density of the solvent, was obtained by dressing up with electron density the site distributions derived from classical theory of liquids. The 3D-RISM theory using the Kovalenko-Hirata (KH) closure[6,47] is used to obtain site distributions.

Using previously reported shifts obtained in explicit simulations for aminocoumarin in water, it is shown that the averaging of the absorption lines corresponding to instantaneous conformations of the solvent can be efficiently replaced by a single evaluation of the excitation energy of solvent molecules in the average embedding potential. In atomistic simulations, the shifts of the lowest-lying $\pi \rightarrow \pi^*$ excitations depend strongly on the number of instantaneous configurations. They were reported to be equal to −0.28 and −0.25 eV for one and eight 50 ps trajectories, respectively.[29] The shift obtained in the present work, which involves only one evaluation of the excitation energy of the solvated molecule, amounts to −0.25 eV, which is in remarkable agreement with the results of the atomistic simulations. A similar agreement between results obtained with the orbital-free embedding potential but with and without the approximation concerning the averaging procedure introduced in this work was found for solvatochromic shifts of the acetone in water. Abandoning the explicit level of description of the solvent makes it, however, impossible to get the shape of the absorption band. Only the position of the maximum of each band maximum can be evaluated. The accuracy of the calculated spectral shifts depends primarily on the accuracy of the method used to calculate the excitation energy shifts at a given geometry of the environment (based on the combination of the linear-response time-dependent density functional theory LR-TDDFT and orbital-free embedding[39,40] in the present case). Our benchmarking studies on hydrogen-bonding induced spectral shifts for similar systems[22,40] indicate that such error is in the range of 0.02−0.05 eV. Taking as the study case, the spectral shifts for the $n \rightarrow \pi^*$ excitations for acetone in solvents of various hydrogen-bonding properties (water, methanol, diethyl ether, n-hexane) shows that the method used to account for solvent structural flexibility does not lead to deterioration of the quality of the calculated shifts. For these solvents, the discrepancies between the calculated and measured maxima of the absorption bands in liquid phase are in the range of 0.04 eV (or smaller). These rather small errors can be thus attributed to the intrinsic accuracy of the applied method to calculate spectral shifts at a rigid geometry. For the ensemble of the studied chromophores and solvents, the calculated solvatochromic shifts agree rather well with experimental measurements. In the worst case, that is, $n \rightarrow \pi^*$ excitation for benzophenone in water, the calculations reproduce 50% of the experimental shifts (−0.10 vs −0.20 eV). This underestimation is probably due to the approximation made in eq 7 that neglects the instantaneous coupling between the induced dipole moment of the chromophore and the structure of the solvent, which is averaged out in the applied method. In the absence of such coupling, the contributions to the absorption band due to such configurations of the solvent which generate strong electric field are underrepresented.

The proposed strategy to evaluate the solvatochromic shifts fails, however, to describe the increase of the magnitude of the experimental shift in the $\pi \rightarrow \pi^*$ transition in aminocoumarin C151 from −0.22 to −0.31 eV when going from water to methanol. Whereas the calculated spectral shift in water is rather good (−0.25 eV), it is underestimated in methanol (−0.21 eV).

The applied approach offers significant computational saving due to replacing a great number of evaluations of the excitation energy at different embedding potentials (one for each solvent configurations) by one evaluation of the excitation energy but with the average embedding potential. The possible savings are proportional to the number of configurations used in the statistical ensemble. This might depend on the system and on technique to generate the instantaneous geometries for the statistical ensemble but can be expected in the order of 1000 configurations at least. Additional savings are possible due to the fact that the generation of the averaged electron density from dressed up 3D-RISM site distributions is faster than explicit evaluation of the frozen electron density of solvent molecules. Note that a number of simplifications can be applied for this purpose in atomistic simulations.[28,29]

Finally, it is worthwhile to underline that the orbital-free embedding potential of Wesolowski and Warshel, similarly to most of the embedding potentials reported in the literature, comprises the electrostatic component. It comprises, however, also the nonelectrostatic terms derived in the exact embedding theory.[13,14,18] These terms are not given as exact analytic expressions because such expressions are not known. They are evaluated by means of some approximants to the exact density functionals. The numerical results obtained with neglecting nonelectrostatic components in the exact embedding potential are included in the present work for comparison purposes. They indicate that nonelectrostatic terms lead typically to improved agreement between calculated and measured spectral shifts, although the nonelectrostatic components of the embedding potential lead to negligible effect on the excitation energies in some cases. It should be underlined that the nonelectrostatic terms in the orbital-free embedding potential (eq 1) ensure that the embedded orbitals (occupied and nonoccupied) are obtained from variational calculations. In practice, it manifests itself by the fact that their shapes and energies depend less on the choice of the basis set used to construct the embedded orbitals than in the electrostatic-only case[30,40,73,141]

Acknowledgment. This work was supported by the grant 200020-124817 from the Fonds National Suisse de la Recherche Scientifique and by the National Research Council (NRC) of Canada. J.W.K. is grateful to the National Institute for Nanotechnology (NINT) for the hospitality during his stay there.

Note Added after ASAP Publication. This article posted ASAP on April 26, 2010. Equations 11 and 12 are revised. The correct version posted on April 30, 2010.

References and Notes

(1) Reichardt, C. *Chem. Rev.* **1994**, *94*, 2319.
(2) Tomasi, J.; Mennucci, B.; Cammi, R. *Chem. Rev.* **2005**, *105*, 2999.
(3) Tomasi, J. *Theor. Chem. Acc.* **2004**, *112*, 184.
(4) Svensson, M.; Humbel, S.; Froese, R. D. J.; Matsubara, T.; Sieber, S.; Morokuma, K. *J. Phys. Chem.* **1996**, *100*, 19357.
(5) Warshel, A.; Levitt, M. *J. Mol. Biol.* **1976**, *103*, 227.
(6) Kovalenko, A. Three-dimensional RISM theory for molecular liquids and solid-liquid interfaces. In: Hirata, F. *Molecular Theory of Solvation: Understanding Chemical Reactivity*; Kluwer Acedemic Publishers: Dordrecht, The Netherlands, 2003; Vol *24*, pp 169−275; and references therein.
(7) Jensen, L.; van Duiknen, P. T.; Snijders, J. G. *J. Chem. Phys.* **2003**, *118*, 514.
(8) Jensen, L.; van Duiknen, P. T.; Snijders, J. G. *J. Chem. Phys.* **2003**, *119*, 3800.
(9) Thole, B. T.; van Duijnen, P. T. *Theor. Chim. Acta* **1980**, *55*, 307.
(10) Sauer, J.; Ugliengo, P.; Garrone, E.; Sounders, V. *Chem. Rev.* **1994**, *94*, 2095.
(11) Gao, J. Methods and applications of combined quantum mechanical and molecular mechanical potentials. In *Reviews in Computational Chemistry*; Lipkowitz, K. B. Boyd, D. B. Eds.; VCH Publishers: New York, 1996; Vol *7*, p 119.
(12) Wesolowski, T. A.; Warshel, A. *J. Phys. Chem.* **1993**, *97*, 8050.
(13) Wesolowski, T. A. *Phys. Rev. A* **2008**, *77*, 012504.
(14) Pernal, K.; Wesolowski, T. A. *Int. J. Quantum Chem.* **2009**, *109*, 2520.
(15) Hohenberg, P.; Kohn, W. *Phys. Rev.* **1964**, *136*, B864.
(16) Kohn, W.; Sham, L. J. *Phys. Rev.* **1965**, *140*, A1133.
(17) Levy, M. *Proc. Natl. Acad. Sci. U. S. A.* **1979**, *76*, 6062.
(18) *One-Electron Equations for Embedded Electron Density: Challenge for Theory and Practical Payoffs in Multi-Level Modelling of Soft Condensed Matter*; Leszczynski, J., Ed.; World Scientific: 2006; Vol *X*, p 1.
(19) Gomes, A. S. P.; Jacob, C. R.; Visscher, L. *Phys. Chem. Chem. Phys.* **2008**, *10*, 5353.
(20) Kluner, T.; Govind, N.; Wang, Y. A.; Carter, E. A. *J. Chem. Phys.* **2002**, *116*, 42.
(21) Lahav, D.; Kluner, T. *J. Phys., Cond. Matt.* **2007**, *19*, 226001.
(22) Fradelos, G.; Kaminski, J. W.; Wesolowski, T. A.; Leutwyler, S. *J. Phys. Chem. A* **2009**, *113*, 9766.
(23) Dreuw, A.; Head-Gordon, M. *Chem. Rev.* **2006**, *105*, 4009.
(24) Klamt, A. *J. Phys. Chem.* **1996**, *100*, 3349.
(25) Hernandes, M. Z.; Longo, R.; Coutinho, K.; Canuto, S. *Phys. Chem. Chem. Phys.* **2004**, *6*, 2088.
(26) Baranovski, V. I. *Opt. Spectrosc.* **2007**, *103*, 540.
(27) Fortrie, R.; Chermette, H. *Theor. Chem. Acc.* **2008**, *120*, 363.
(28) Neugebauer, J.; Louwerse, M. J.; Baerends, E. J.; Wesolowski, T. A. *J. Chem. Phys.* **2005**, *122*, 094115.
(29) Neugebauer, J.; Jacob, C. R.; Wesolowski, T. A.; Baerends, E. J. *J. Phys. Chem. A* **2005**, *109*, 7805.
(30) Zbiri, M.; Atanasov, M.; Daul, C.; Garcia-Lastra, J. M.; Wesolowski, T. A. *Chem. Phys. Lett.* **2004**, *397*, 441.
(31) Fdez Galván, I.; Sánchez, M. L.; Martín, M. E.; Olivares del Valle, F. J.; Aguilar, M. A. *Comp. Phys. Comm.* **2003**, *155*, 244.
(32) Coutinho, K.; Georg, H. C.; Fonseca, T. L.; Ludwig, V.; Canuto, S. *Chem. Phys. Lett.* **2007**, *437*, 148.
(33) Kongsted, J.; Osted, A.; Mikkelsen, K. V.; Christiansen, O. *J. Chem. Phys.* **2003**, *118*, 1620.
(34) Wesolowski, T.; Warshel, A. *J. Phys. Chem.* **1994**, *98*, 5183.
(35) Cortona, P. *Phys. Rev. B* **1991**, *44*, 8454.
(36) Wesolowski, T. A.; Weber, J. *Chem. Phys. Lett.* **1996**, *248*, 71.
(37) Aidas, K.; Kongsted, J.; ad, K. V.; Mikkelsen, A. O.; Christiansen, O. *J. Phys. Chem. A* **2005**, *109*, 8001.
(38) Besley, N. A.; Oakley, M. T.; Cowan, A. J.; Hirst, J. D. *J. Am. Chem. Soc.* **2004**, *126*, 13502.
(39) Casida, M. E.; Wesolowski, T. A. *Int. J. Quantum Chem.* **2004**, *96*, 577.
(40) Wesolowski, T. A. *J. Am. Chem. Soc.* **2004**, *126*, 11444.
(41) Car, R.; Parrinello, M. *Phys. Rev. Lett.* **1985**, *55*, 2471.
(42) Magyar, R. J.; Tretiak, S. *J. Chem. Theory and Comput.* **2007**, *3*, 976.
(43) Tawada, Y.; Tsuneda, T.; Yanagisawa, S.; Yanai, T.; Hirao, K. *J. Chem. Phys.* **2004**, *120*, 8425.
(44) Dreuw, A.; Head-Gordon, M. *J. Am. Chem. Soc.* **2004**, *126*, 4007.
(45) van Gisbergen, S. J. A.; Schipper, P. R. T.; Gritsenko, O. V.; Baerends, E. J. *Phys. Rev. Lett.* **1999**, *83*, 694.
(46) Neugebauer, J. *J. Chem. Phys.* **2007**, *97*, 134116.
(47) Kovalenko, A.; Hirata, F. *J. Chem. Phys.* **1999**, *110*, 10095.
(48) Hansen, J. P.; McDonald, I. R. *Theory of Simple Liquids*, 2nd ed.; Academic: London, 1986.
(49) Perkyns, J. S.; Pettitt, B. M. *Chem. Phys. Lett.* **1992**, *97*, 7656.
(50) Kovalenko, A.; Hirata, F. *Chem. Phys. Lett.* **2001**, *349*, 496.
(51) Kovalenko, A.; Hirata, F. *J. Theor. Comput. Chem.* **2002**, *1*, 381.
(52) Yoshida, K.; Yamaguchi, T.; Kovalenko, A.; Hirata, F. *J. Phys. Chem. B* **2002**, *106*, 5042.
(53) Omelyan, I.; Kovalenko, A.; Hirata, F. *J. Theor. Comput. Chem.* **2003**, *2*, 193.
(54) Yamazaki, T.; Imai, T.; Hirata, F.; Kovalenko, A. *J. Phys. Chem. B* **2007**, *111*, 1206.
(55) Yoshida, N.; Imai, T.; Phongphanphanee, S.; Kovalenko, A.; Hirata, F. *J. Phys. Chem. B* **2009**, *113*, 873.
(56) Imai, T.; Kovalenko, A.; Hirata, F.; Kidera, A. *J. Interdiscip. Sci: Comput. Life Sci.* **2009**, *1*, 156.
(57) Imai, T.; Oda, K.; Kovalenko, A.; Hirata, F.; Kidera, A. *J. Am., Chem. Soc.* **2009**, *131*, 12430.
(58) Yamazaki, T.; Kovalenko, A.; Murashov, V. V.; Patey, G. N. *J. Phys. Chem. B* **2010**, *114*, 613.
(59) Kovalenko, A.; Hirata, F. *J. Chem. Phys.* **2000**, *112*, 10391.
(60) Kovalenko, A.; Hirata, F. *J. Chem. Phys.* **2000**, *112*, 10403.
(61) Chandler, D.; Andersen, H. C. *J. Chem. Phys.* **1972**, *57*, 1930.
(62) Hirata, F.; Rossky, P. *Chem. Phys. Lett.* **1981**, *83*, 329.

(63) Hirata, F.; Pettitt, B. M.; Rossky, P. *J. Chem. Phys.* **1982**, *77*, 509.
(64) Hirata, F.; Rossky, P.; Pettitt, B. M. *J. Chem. Phys.* **1983**, *78*, 4133.
(65) Chandler, D.; McCoy, J.; Singer, S. *J. Chem. Phys.* **1986**, *85*, 5971.
(66) Chandler, D.; McCoy, J.; Singer, S. *J. Chem. Phys.* **1986**, *85*, 5977.
(67) Beglov, D.; Roux, B. *J. Phys. Chem. B* **1997**, *101*, 7821.
(68) Chandler, D.; McCoy, J. D.; Singer, S. J. *J. Chem. Phys.* **1986**, *85*, 5971–5977.
(69) Singer, S. J.; Chandler, D. *Mol. Phys.* **1985**, *55*, 621.
(70) Allen,. M. P.; Tildesley, D. J. *Computer Simulation of Liquids*; Oxford University Press: 1987.
(71) Gusarov, S.; Ziegler, T.; Kovalenko, A. *J. Phys. Chem. A* **2006**, *110*, 6083.
(72) Casanova, D.; Gusarov, S.; Kovalenko, A.; Ziegler, T. *J. Chem. Theory Comput.* **2007**, *3*, 458.
(73) Garcia-Lastra, J. M.; Kaminski, J. W.; Wesolowski, T. A. *J. Chem. Phys.* **2008**, *129*, 074107.
(74) Parr, R. G.; Yang, W. *Density-Functional Theory of Atoms and Molecules*; Oxford: New York, 1989.
(75) von Lilienfield, O. A.; Tuckerman, M. A. *J. Chem. Phys.* **2006**, *125*, 154104.
(76) Baerends, E. J. Autschbach, J. Bèrces, A. Bickelhaupt, F. M. Bo, C. Boerrigter, P. M. Cavallo, L. Chong, D. P. Deng, L. Dickson, R. M. Ellis, D. E. van Faassen, M. Fan, L. Fischer, T. H. Fonseca Guerra, C. van Gisbergen, S. J. A. Gotz, A. W. Groeneveld, J. A. Gritsenko, O. V. Grüning, M. Harris, F. E. van den Hoek, P. Jacob, C. R. Jacobsen, H. Jensen, L. van Kessel, G. Kootstra, F. Krykunov, M. V. van Lenthe, E. McCormack, D. A. Michalak, A. Neugebauer, J. Nicu, V. P. Osinga, V. P. Patchkovskii, S. Philipsen, P.H. T. Post, D. Pye, C. C. Ravenek, W. Rodriguez, J. I. Ros, P. Schipper, P. R. T. Schreckenbach, G. Snijders, J. G. Sol'a, M. Swart, M. Swerhone, D. te Velde, G. Vernooijs, P. Versluis, L. Visscher, L. Visser, O. Wang, F. Wesolowski, T. A. van Wezenbeek, E. M. Wiesenekker, G. Wolff, S. K. Woo, T. K. Yakovlev, A. L. Ziegler, T. *ADF2008.01, SCM, Theoretical Chemistry*; Vrije Universiteit: Amsterdam, The Netherlands, 2008; http://www.scm.com.
(77) Jacob, C. R.; Neugebauer, J.; Visscher, L. *J. Comput. Chem.* **2008**, *29*, 1011.
(78) Swart, M.; van Duijnen, P. T.; Snijders, J. G. *J. Comput. Chem.* **2001**, *22*, 79.
(79) Dirac, P. A. M. *Proc. Cambridge Philos. Soc.* **1930**, *26*, 376.
(80) Ceperley, D. M.; Alder, B. J. *Phys. Rev. Lett.* **1980**, *45*, 566.
(81) Vosko, S. H.; Wilk, L.; Nusair, M. *Can. J. Phys.* **1980**, *58*, 1200.
(82) Jorgensen, W. L.; Maxwell, D. S.; Tirado-Rives, J. *J. Am. Chem. Soc.* **1996**, *118*, 11225.
(83) Jorgensen, W. L.; Madura, J. D.; Swenson, C. J. *J. Am. Chem. Soc.* **1984**, *106*, 6638.
(84) Becke, A. D. *Phys. Rev. A* **1988**, *38*, 3098.
(85) Perdew, J. P. *Phys. Rev. B* **1986**, *33*, 8822.
(86) Thomas, L. H. *Proc. Cambridge Philos. Soc.* **1927**, *23*, 542.
(87) Fermi, E. *Z. Phys.* **1928**, *48*, 73.
(88) Schipper, P.; Gritsenko, O.; van Gisbergen, S.; Baerends, E. *J. Chem. Phys.* **2000**, *112*, 1344.
(89) Gritsenko, O. V.; Schipper, P. R. T.; Baerends, E. J. *Chem. Phys. Lett.* **1999**, *302*, 199.
(90) Wesolowski, T. A.; Chermette, H.; Weber, J. *J. Chem. Phys.* **1996**, *105*, 9182.
(91) Gustavsson, T.; Cassara, L.; Gulbinas, V.; Gurzadyan, G.; Pommeret, J.-C.; Sorguis, M.; van der Meulen, P. *J. Phys. Chem. A* **1998**, *102*, 4229.
(92) Moylan, C. R. *J. Phys. Chem.* **1994**, *98*, 13513.
(93) Jones, G. II; Jackson, W. R.; Choi, C.; Bergmark, W. R. *J. Phys. Chem.* **1985**, *89*, 294.
(94) Dulak, M.; Kaminski, J. W.; Wesolowski, T. A. *Int. J. Quantum Chem.* **2009**, *109*, 1886.
(95) Sulpizi, M.; Carloni, P.; Hutter, J.; Rothlisberger, U. *Phys. Chem. Chem. Phys.* **2003**, *5*, 4798.
(96) Cave, R. J.; Burke, K.; Castner, E. W., Jr. *J. Phys. Chem. A* **2002**, *106*, 9294.
(97) Klamt, A.; Shuurmann, G. *J. Chem. Soc. Trans.* **1993**, *2*, 799.
(98) Pavone, M.; Crescenzi, O.; Morelli, G.; Rega, N.; Barone, V. *Theor. Chem. Acc.* **2006**, *116*, 1456.
(99) Bernasconi, L.; Sprik, M.; Hutter, J. *Chem. Phys. Lett.* **2004**, *394*, 141.
(100) Aquilante, F.; Cossi, M.; Crescenzi, O.; Scalmani, G.; Barone, V. *Mol. Phys.* **2003**, *101*, 1945.
(101) Rohrig, U. F.; Frank, I.; Hutter, J.; Laio, A.; VandeVondele, J.; Rothlisberger, U. *PhysChemPhys* **2003**, *4*, 1177.
(102) Coutinho, K.; Canuto, S. *THEOCHEM* **2003**, *632*, 235.
(103) Coutinho, K.; Saavedra, N.; Canuto, S. *THEOCHEM* **1999**, *466*, 69.
(104) Grozema, F. C.; van Duijnen, P. T. *J. Phys. Chem. A* **1998**, *102*, 7984.
(105) de Vries, A. H.; van Duijnen, P. T. *Int. J. Quantum Chem.* **1996**, *57*, 1067.
(106) Ten-no, S.; Hirata, F.; Kato, S. *J. Chem. Phys.* **1994**, *100*, 7443.
(107) Fox, T.; Rosch, N. *Chem. Phys. Lett.* **1992**, *191*, 33.
(108) Porter, C. W.; Iddings, C. *J. Am. Chem. Soc.* **1926**, *48*, 40.
(109) Bayliss, N. S.; McRae, E. G. *J. Chem. Phys.* **1954**, *58*, 1006.
(110) Bayliss, N. S.; Wills-Johnson, G. *Spectrochim. Acta, Part A* **1968**, *24*, 551.
(111) Hayes, W. P.; Timmons, C. J. *Spectrochim. Acta* **1965**, *21*, 529.
(112) Balasubramanian, A.; Rao, C. N. R. *Spectrochim. Acta* **1962**, *18*, 1337.
(113) Suppan, P. *J. Photochem. Photobiol. A* **1990**, *50*, 293.
(114) Renge, I. *J. Phys. Chem. A* **2009**, *113*, 10678.
(115) Aidas, K.; Mogelhoj, A.; Nilsson, E. J. K.; Johnson, M. S.; Mikkelsen, K. V.; Christiansen, O.; Soderhjelm, P.; Kongsted, J. *J. Chem. Phys.* **2008**, *128*, 194503.
(116) Becker, R. S.; Inuzuka, K.; King, J. *J. Chem. Phys.* **1970**, *52*, 5164.
(117) Moskvin, A. F.; Yablonski, O. P.; Bodnar, I. F. *Theor. Exp. Chem.* **1966**, *22*, 469.
(118) Inuzuka, K. *Bull. Chem. Soc. Jpn.* **1961**, *34*, 6.
(119) Inuzuka, K. *Bull. Chem. Soc. Jpn.* **1960**, *33*, 678.
(120) Forbes, W. F.; Shilton, R. *J. Am. Chem. Soc.* **1959**, *81*, 786.
(121) Mackinney, G.; Temmer, O. *J. Am. Chem. Soc.* **1948**, *70*, 3286.
(122) Walsh, A. D. *Trans. Faraday. Soc.* **1945**, *41*, 498.
(123) Buswell, A. M.; Dunlop, E. C.; Rodebush, W. H.; Swartz, J. B. *J. Am. Chem. Soc.* **1940**, *62*, 325.
(124) Blacet, F. E.; Young, W. G.; Roof, J. G. *J. Am. Chem. Soc.* **1937**, *59*, 608.
(125) Eastwood, E.; Snow, C. P. *Proc. R. Soc. London, Ser. A* **1935**, *149*, 446.
(126) Luthy, A. *Z. Phys. Chem.* **1923**, *107*, 284.
(127) Losa, A. M.; Fdez-Galván, I.; Aguilar, M. A.; Martín, M. E. *J. Phys. Chem. B* **2007**, *111*, 9864.
(128) Brancato, G.; Rega, N.; Barone, V. *J. Chem. Phys.* **2006**, *125*, 164515.
(129) Georg, H. C.; Coutinho, K.; Canuto, S. *J. Chem. Phys.* **2005**, *123*, 124307.
(130) Martín, M. E.; Losa, A. M.; Fdez-Galván, I.; Aguilar, M. A. *J. Chem. Phys.* **2004**, *121*, 3710.
(131) Monte, S. A.; Muller, T.; Dallos, M.; Lischka, H.; Diedenhofen, M.; Klamt, A. *Theor. Chem. Acc.* **2004**, *111*, 78.
(132) Aquilante, F.; Barone, V.; Roos, B. O. *J. Chem. Phys.* **2003**, *119*, 12323.
(133) Dilling, W. L. *J. Org. Chem.* **1966**, *31*, 1045.
(134) Georg, H. C.; Coutinho, K.; Canuto, S. *J. Chem. Phys.* **2007**, *126*, 034507.
(135) Urahata, S.; Canuto, S. *Int. J. Quantum Chem.* **2000**, *80*, 1062.
(136) Fattebert, J.-L.; Law, R. J.; Bennion, B.; Lau, E. Y.; Schwegler, E.; Lightstone, F. C. *J. Chem. Theory Comput.* **2009**, *5*, 2257.
(137) Laio, A.; VandeVondele, J.; Rothlisberger, U. *J. Chem. Phys.* **2002**, *116*, 6941.
(138) Ten-no, S.; Hirata, F.; Kato, S. *Chem. Phys. Lett.* **1993**, *214*, 391.
(139) Sato, H.; Hirata, F.; Kato, S. *J. Chem. Phys.* **1996**, *105*, 1546.
(140) Dulak, M.; Wesolowski, T. A. *J. Chem. Phys.* **2006**, *124*, 164101.
(141) Wesolowski, T. A.; Weber, J. *Int. J. Quantum Chem.* **1997**, *61*, 303.

JP100158H